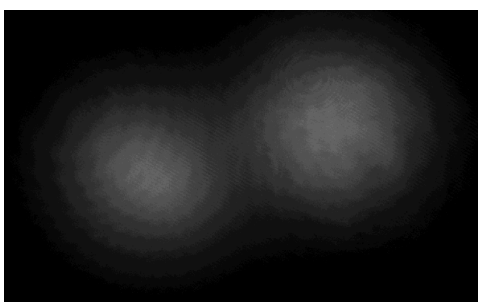




Quantum entangled single photons with partial distinguishability



THESIS

submitted in partial fulfillment of the
requirements for the degree of

MASTER OF SCIENCE

in

PHYSICS AND BUSINESS STUDIES

Author :

Student ID :

Supervisor :

2nd corrector :

Gerard Westra

s1298275

Dr. W. Löffler

Dr. V. Dunjko

Leiden, The Netherlands, July 25, 2019

Quantum entangled single photons with partial distinguishability

Gerard Westra

Huygens-Kamerlingh Onnes Laboratory, Leiden University
P.O. Box 9500, 2300 RA Leiden, The Netherlands

July 25, 2019

Abstract

This thesis gives insight into two photon quantum interference effects in quantum optics, with Hong-Ou-Mandel visibility detection. This is studied using a delay loop with different light polarizations. The single photons are created by exciting a quantum dot in a microcavity with a continuous-wave laser. We try to relate experimental results of the second order correlation function to a theoretical analysis of the obtained photon states in the system. As a result an insight into the creation of highly entangled qubit states, called cluster states, is given.

Contents

1	Introduction	1
1.1	Background	1
1.2	Goal	3
2	Quantum optics and indistinguishability	5
2.1	Quantum mechanical introduction	5
2.1.1	Quantum optics	6
2.1.2	Two-particle configuration	8
2.1.3	(In)distinguishable elementary particles	9
2.2	The Gibbs paradox	10
2.2.1	Description of the problem	11
2.2.2	Solution of the problem	12
2.3	Electromagnetic radiation	13
2.3.1	Thermal light	13
2.3.2	Coherent light	15
2.4	Degree of indistinguishability	15
2.4.1	Description of single photons	15
2.4.2	Classical beam splitter	17
2.4.3	Quantum beam splitter	18
2.4.4	Two-photon interference, polarization degree of freedom	19
2.4.5	Two-photon interference, temporal degree of freedom	20
3	Experimental setup	23
3.1	Contents of the optical setup	23
3.2	Polarization in the optical setup	25
4	Photon interference and bunching	27
4.1	Interference visibility	27
4.1.1	Example: measurement of the visibility	28
4.2	Hanbury Brown and Twiss effect	28

4.3	Hanbury Brown and Twiss experiment	30
4.4	Alignment of the setup	31
4.5	Normalization fit	32
5	Spatial alignment	37
5.1	“No loop” setup	37
5.1.1	“No loop” prediction	37
5.1.2	“No loop” experiment	38
5.2	Delay loop setup (one round trip R)	40
5.2.1	Delay loop (one round trip R) prediction	42
5.2.2	Delay loop (one round trip R) experiment	43
6	Cluster States and indistinguishability	49
6.1	Cluster states	49
6.2	Cluster state setup prediction	51
6.2.1	Method	51
6.2.2	Single photon input (red operator in loop)	53
6.2.3	Two photon input with 2 round trips (red operator in loop)	54
6.2.4	Prediction after 3 round trips	55
6.3	Cluster state setup experiment 1	56
6.4	Cluster state setup experiment 2	58
7	Conclusion	61
7.1	Research questions	61

Introduction

This thesis reports the research in the Quantum Optics group led by Dr. W. Löffler from Leiden University in the Netherlands. This group is part of the Leiden Institute of Physics (LION) and research has taken place at the Huygens Laboratory between February and August 2019.

1.1 Background

The focus of this work lies on the distinguishability of photons when they become highly entangled cluster states for computational tasks. Quantum entanglement between photons is a non local effect where the state of one photon state depends on the measurement outcome of the other state. An interesting case is the Bell state which consists of two entangled qubits. These qubits can be used for physical implementations of quantum information processing with two-state photonic systems. The degree of freedom for this system is the polarization of light, described by two optical modes: horizontal and vertical. Single photons can be in a superposition of these two polarization modes.

A light beam can be described as a classical wave and as a quantum stream of photons. In principle single photons are identical if they are indistinguishable, so they can undergo quantum interference at, e.g., a beam splitter. These single photons are in contrast with laser light (**L**ight **A**mplification by **S**timulated **E**mission of **R**adiation), see appendix ??, which creates single-mode light. Light coming out from a laser is coherent light, which is different for other light sources, such as white light.

Our setup, to generate the entangled cluster states from a single photon quantum dot source, is similar to the one proposed in Pilnyak et al. [30] and to the Mach-Zehnder-interferometer-like setup proposed by Patel et al. [29] and Proux et al. [32]. This setup consist of various optical elements, among which are a (polarizing) beam splitter and waveplates. For this research we need to generate highly indistinguishable photons,

so here is a short historical overview of the research on indistinguishable particles and single photons:

Year	Scientists	Development
1876	J.W. Gibbs	Particles need to be indistinguishable due to the Gibbs paradox [17].
1901	M.K.E.L. Planck	Electromagnetic waves are quantized in packets of energy [31].
1905	A. Einstein	Light is quantized in localized photons [9].
1954	P.A.M. Dirac	Indistinguishable photons can be interchanged without an observable change [8].
1956	R. Hanbury Brown et al.	Measuring an interference effect between two signals, in their Hanbury Brown and Twiss setup, with which they determined the angular diameter of Sirius [14].
1965	A.M.L. Messiah et al.	Indistinguishable classical and quantum mechanical particles have the same physical properties [26].
1966	J.M. Jauch	Indistinguishable quantum mechanical particles have the same intrinsic physical properties. Classical particles are distinguishable. [16].
1973	R. Mirman	Classical and quantum mechanical particles that are far apart and have a distinguishable motion are distinguishable [27].
1987	C. K. Hong, Z. Y. Ou and L. Mandel	Demonstration of quantum interference with the Hong-Ou-Mandel effect. Distinguishability of photons is therefore related to the probability of detection. With parametric down-conversion indistinguishable photons are produced [15].
1991	L. Mandel	Quantum interference between two light waves in an interferometer is related to the degree of indistinguishability of the paths, which is equal to the degree of coherence. This has been shown by decomposition of the density operator [23].
2002	C. Santori et al.	Indistinguishable single photons can be created from a single photon source and interaction between these photons can be calculated with a mean quantum wave-packet overlap M [33].
2008	R. B. Patel et al.	The effect of parallel and orthogonal polarization input in the Hanbury Brown and Twiss setup can be examined with a Mach-Zehnder-Interferometer. [29].
2012	R. M. Stevenson et al.	Indistinguishable entangled single photons can be created from a pair of photons, coming from a quantum dot source, with a simultaneously emitted photon from an independent pair of photons from this source. [35].
2015	R. Proux et al.	The temporal indistinguishability of single photons by continuous wave excitation of the quantum dot can be measured. [32].
2017	Y. Pilnyak et al.	Measurements with indistinguishable photons with a photonic cluster state setup [30].

1.2 Goal

The goal of this thesis is to answer the following research question:

What is the effect of partial distinguishable single photons and first order interference in a loop setup designed for the creation of cluster states?

This question is subdivided into:

- How does a change in the properties of the quantum optical single photon source affect the indistinguishability?
- Which consequences does a spatial or temporal misalignment have on the quantum interference in the cluster state loop setup?
- What impact have partial distinguishable single photons on the quantum information processing with quantum entangled qubits in cluster states?

The first section of this thesis is about imperfections from the single photon source. An experiment is executed to determine photon number purity. Then we discuss the partial distinguishability of photons and quantum interference. The wave function overlap between paths is discussed. We build the setup step by step, from the Hanbury Brown and Twiss setup until we finally reach the setup we use to generate cluster states. Research is done in partial collaboration with Edward Hissink (Leiden University).

Quantum optics and indistinguishability

In this chapter we study subjects from Quantum Optics, with an emphasis on the different types of light sources and we also introduce the need for the indistinguishability of single photons in classical mechanics, see the Gibbs paradox. Furthermore the effects of the beam splitter and two-photon quantum interference is discussed.

2.1 Quantum mechanical introduction

In Quantum Mechanics a quantum system can be described by a quantum wave function or quantum state. We represent quantum states as vectors in Hilbert space. In order to experimentally access the quantum states observables are introduced. Examples of observables include position and momentum. Observables are represented as operators with corresponding eigenvalues.

Adding states together is described by the superposition principle for states. Here pure quantum states are described in bra-ket notation. Mixed states on the other hand can only be described by density matrices, which consists of multiple pure states. An example of superposition of any linear combination for pure states $|A\rangle$ and $|B\rangle$ equal to $|\Psi\rangle$ state in bra-ket notation is given by: [25]

$$|\Psi\rangle = c_A |A\rangle + c_B |B\rangle, \quad (2.1)$$

with arbitrary complex numbers:

$$c_{A,B} \in \mathbb{C}. \quad (2.2)$$

This is an example of a two-state quantum system. For a probability distribution the normalization condition is needed to describe a physical state in Hilbert space:

$$\langle\Psi|\Psi\rangle = 1. \quad (2.3)$$

Since the length of vectors now has no meaning due to normalization, the quantum states we consider are part of the projective Hilbert Space. In order to describe the

probability of finding results of a measurement we first look at a generic quantum state: [3]

$$|\Psi\rangle = \sum_n c_n |\Psi_n\rangle, \quad (2.4)$$

where we sum over n quantum states and $|\Psi_n\rangle$ is the eigenfunction of $|\Psi\rangle$. Now the probability of finding a state $|\Psi_n\rangle$ in the state of equation 2.4 is given by: [18]

$$P_n = |\langle \Psi_n | \Psi \rangle|^2 = |c_n|^2. \quad (2.5)$$

Because of orthogonality and the normalization condition the total probability thus is, as expected:

$$\sum_n P_n = 1. \quad (2.6)$$

This was a brief discussion about the quantum mechanical and mathematical prerequisites needed to read this thesis. If you want to read a more comprehensive introduction we recommend the books from K. Konishi & G. Paffuti [18] and L.E. Ballentine [2].

2.1.1 Quantum optics

Light can be quantized in photons which could be described by:

- number states $|n_{k_i}\rangle$ (Fock space), with the occupation number $n \in \mathbb{Z}$. A photon is an excitation of a normal mode k_i . This depends on the radiation pattern of the electromagnetic field or the structure and boundary conditions of the photon.
- polarization states $|P\rangle$ (mode space), with the polarization P .

In the next paragraphs we switch between these states. We consider here only the fundamental Gaussian transverse mode. The energy of a photon in an electromagnetic mode is, also known as the Planck-Einstein relation [11],

$$E_{k_i} = h\omega, \quad (2.7)$$

with h the Planck constant and ω the photon's frequency. Now in Fock space, we write the basis of an electromagnetic field as:

$$|\Psi_{EM}\rangle = |n_{k_0}\rangle \otimes |n_{k_1}\rangle \otimes \dots \otimes |n_{k_j}\rangle, \quad (2.8)$$

where the \otimes is the tensor product used to describe the total Hilbert space of the interacting particles. If an electromagnetic wave oscillates in one direction it is called linear polarization. An example of the usage of tensor products using linearly polarized light:

Example: tensor product between two subsystems

The tensor product between two quantum systems with horizontal $|H\rangle$ and vertical polarization $|V\rangle$ is discussed:

$$|H\rangle = \begin{bmatrix} 1 \\ 0 \end{bmatrix}, \quad (2.9)$$

$$|V\rangle = \begin{bmatrix} 0 \\ 1 \end{bmatrix}, \quad (2.10)$$

$$|H\rangle \otimes |V\rangle = \begin{bmatrix} 0 \\ 1 \\ 0 \\ 0 \end{bmatrix}. \quad (2.11)$$

Using the following subsystems,

$$|\Psi_A\rangle = \frac{1}{\sqrt{2}} (|H\rangle + |V\rangle), \quad (2.12)$$

$$|\Psi_B\rangle = |H\rangle. \quad (2.13)$$

the tensor products between these systems in Hilbert spaces $H_A \otimes H_B$ and $H_B \otimes H_A$ is given by:

$$|\Psi_A\rangle |\Psi_B\rangle = \frac{1}{\sqrt{2}} (|HH\rangle + |VH\rangle), \quad (2.14)$$

$$|\Psi_B\rangle |\Psi_A\rangle = \frac{1}{\sqrt{2}} (|HH\rangle + |HV\rangle), \quad (2.15)$$

where we introduced a notation to shorten the equations:

$$|i\rangle \otimes |j\rangle = |i\rangle |j\rangle = |i,j\rangle = |ij\rangle. \quad (2.16)$$

Here we see that the order of the tensor product is important.

As usual, we have the raising \hat{a}^\dagger and lowering operators \hat{a} [12]. When these operators act on Fock state $|n\rangle$ they can create or annihilate a photon.

$$\hat{a}^\dagger |n\rangle = \sqrt{n+1} |n+1\rangle, \quad (2.17)$$

$$\hat{a} |n\rangle = \sqrt{n} |n-1\rangle, \quad (2.18)$$

with $n \in \mathbb{Z}$. One harmonic oscillator then looks like:

$$|n\rangle = \frac{(\hat{a}^\dagger)^n}{\sqrt{n!}} |0\rangle. \quad (2.19)$$

And several harmonic oscillators, using equation 2.8 would then look like:

$$|n_0, n_1, \dots, n_j\rangle = \frac{1}{\sqrt{n_0 n_1 \dots n_j}} (\hat{a}^\dagger)^{n_0} (\hat{a}^\dagger)^{n_1} \dots (\hat{a}^\dagger)^{n_j} |0, 0, \dots, 0\rangle. \quad (2.20)$$

The photon number of the j -th mode is given by the photon number operator: [12]

$$\hat{N}_j = \hat{a}_j^\dagger \hat{a}_j. \quad (2.21)$$

The quantum systems used in this thesis are photons and thus bosons, which obey the Bose-Einstein statistics we will discuss in a following chapter.

2.1.2 Two-particle configuration

The generic linear combination of basis vectors for the two-particle configuration, using equation 2.2 and 2.8 looks like: [2]

$$|\Psi\rangle = \sum_{A,B} c_{A,B} |A\rangle |B\rangle, \quad (2.22)$$

where

$$\Psi(\mathbf{q}_1, \mathbf{q}_2) = \sum_{A,B} c_{A,B} \langle \mathbf{q}_1 | A\rangle \langle \mathbf{q}_2 | B\rangle. \quad (2.23)$$

To gain insight in the order of the basis vectors we introduce the exchange operator \hat{P} that is both Hermitian and unitary, which does the following:

$$\hat{P} |A\rangle |B\rangle = |B\rangle |A\rangle, \quad (2.24)$$

$$\hat{P} \Psi(\mathbf{q}_1, \mathbf{q}_2) = \Psi(\mathbf{q}_2, \mathbf{q}_1). \quad (2.25)$$

We can find the eigenvalues of the exchange operator by two consecutive exchanges of particles for two particles:

$$(\hat{P})^2 |A, B\rangle = \hat{P} |B, A\rangle = |A, B\rangle, \quad (2.26)$$

resulting in

$$(\hat{P})^2 = I. \quad (2.27)$$

Therefore we only can have symmetric or antisymmetric quantum states:

$$\hat{P} |A, B\rangle = \pm |B, A\rangle. \quad (2.28)$$

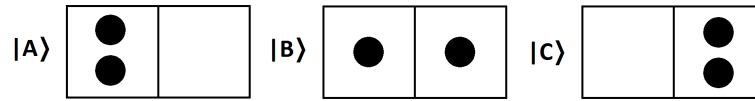


Figure 2.1: Three quantum states represented by two symmetric rectangular boxes with two particles inside illustrated by the filled circles.

2.1.3 (In)distinguishable elementary particles

The spin characteristics of identical particles determine if they form symmetric or antisymmetric quantum states. We now want to see the effect of this property. If the exchange between identical particles is the only difference for two physical situations the particles are indistinguishable. Therefore we take a look at the commutator for bosons (integer spin) and fermions (half-integer spin). The definition for the commutator and anticommutator is given by:

$$[\hat{a}, \hat{b}] = \hat{a}\hat{b} - \hat{b}\hat{a}, \quad (2.29)$$

$$\{\hat{a}, \hat{b}\} = \hat{a}\hat{b} + \hat{b}\hat{a}. \quad (2.30)$$

Bosons exhibit symmetric quantum statistics and fermions exhibit antisymmetric quantum statistics. The commutation relations thus for photons are:

$$[\hat{a}_i, \hat{a}_j] = [\hat{a}_i^\dagger, \hat{a}_j^\dagger] = 0, \quad (2.31)$$

$$[\hat{a}_i, \hat{a}_j^\dagger] = \delta_{i,j} [12]. \quad (2.32)$$

where $\delta_{i,j}$ is the Kronecker delta. In the next example we will look at the effect of distinguishability on particles and quantum states.

Example: Quantum states and indistinguishability

To illustrate the effect of distinguishability we first look at two particles in two different boxes. Each box has its own quantum state in bra-ket notation. Because there is no interaction nor exchange of particles between boxes, only the three different quantum states schematically depicted on figure 2.1 are possible.

- $|A\rangle$: 2 particles in the first box.
- $|B\rangle$: 1 particle in each box.
- $|C\rangle$: 2 particles in the second box.

Here we introduce the particle indistinguishability for bosons and fermions. Since we can view the two boxes as 2 separate quantum states and since two indistinguishable fermions cannot occupy the same quantum state due to the Pauli exclusion principle, state $|A\rangle$ and $|C\rangle$ are for indistinguishable fermions not possible.

For two indistinguishable bosons, the states are equiprobable, with the assumption that the boxes are equal. Now there is only one possible way to describe $|B\rangle$, since it is not possible to tell the difference between the two photons.

For distinguishable particles the spin characteristics do not change the probabilities, and are equal for bosons and fermions. There are now 2 possible ways to describe $|B\rangle$, because switching the particles between the boxes results in the same state.

So we get the following probabilities to measure each quantum state:

	P($ A\rangle$)	P($ B\rangle$)	P($ C\rangle$)
indist. fermions	0	1	0
indist. bosons	1/3	1/3	1/3
dist. particles	1/4	1/2	1/4

We can conclude out of the last example that there are non-classical effects for indistinguishable particles, such as photons. The quantum states look like:

$$|\psi\rangle_{\text{indistinguishable fermions}} = |B\rangle, \quad (2.33)$$

$$|\psi\rangle_{\text{indistinguishable bosons}} = \frac{1}{\sqrt{3}} (|A\rangle + |B\rangle + |C\rangle), \quad (2.34)$$

$$|\psi\rangle_{\text{distinguishable particles}} = \frac{1}{2} (|A\rangle + \sqrt{2}|B\rangle + |C\rangle). \quad (2.35)$$

However, this example does not proof that photons (or other elementary particles) need to be indistinguishable if they are identical. Therefore we need to discuss another example, which is discussed in the next section.

2.2 The Gibbs paradox

The Gibbs paradox [38, 40] is a statistical mechanical statement, proposed by J.W. Gibbs in 1876, in which the indistinguishability of particles needs to be included in the derivation of the entropy. Otherwise the addition of quantum subsystems into a bigger system will give a different entropy than just addition of the entropy of both subsystems together. This would mean that the entropy is not extensive and the second law of thermodynamics is violated. However, the problem is solved if we ignore permutation of particles.

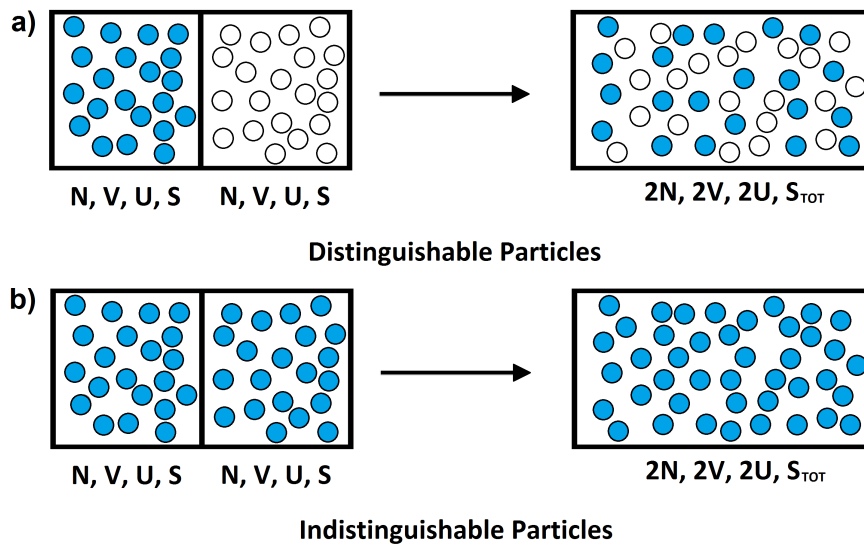


Figure 2.2: Illustration of two compartments separated by a partition which is removed for: a) distinguishable particles, b) indistinguishable particles. Here the number of photons: N , volume: V , total energy: U and entropy: S .

2.2.1 Description of the problem

We have two classical ideal gases in two different compartments. When we remove the partition between the compartments the total entropy of the quantum system is not the same as the sum of the entropy of both compartments. See figure 2.2a for the compartments: the number of photons N , volume V , total energy U and entropy S . Removal of the partition results in a system with the number of photons $2N$, volume $2V$, total energy $2U$ and total entropy S_{TOT} .

The entropy in classical statistical mechanics, with k_B Boltzmann constant and Ω the number of configurations (states), is defined as:

$$S = k_B \ln \Omega. \quad (2.36)$$

Number of states in one compartment: [38, 40]

$$\Omega = c^N V^N \left(\frac{U}{N} \right)^{\frac{3N}{2}}, \quad (2.37)$$

To simplify the expression we set the constant $c = 1$, which consist of other properties of the physical particles. then, the entropy for a single compartment is:

$$S = Nk_B \ln \left(V \left(\frac{U}{N} \right)^{\frac{3}{2}} \right) = Nk_B \left(\ln(V) + \frac{3}{2} \ln \left(\frac{U}{N} \right) \right). \quad (2.38)$$

The total entropy before removal of the partition is $2S$ and after removal:

$$S_{TOT} = 2Nk_B \left(\ln(2V) + \frac{3}{2} \ln \left(\frac{2U}{2N} \right) \right), \quad (2.39)$$

which results in a mixing entropy term with an N dependence:

$$\Delta S = S_{TOT} - 2S \quad (2.40)$$

$$= 2Nk_B \left(\ln(V) + \frac{3}{2} \ln \left(\frac{U}{N} \right) \right) - 2Nk_B \left(\ln(2V) + \frac{3}{2} \ln \left(\frac{2U}{2N} \right) \right) \quad (2.41)$$

$$= 2Nk_B (\ln(V) - \ln(2V)) \quad (2.42)$$

$$= 2Nk_B \ln 2 \neq 0. \quad (2.43)$$

In violation of the second law of thermodynamics, $\Delta S = 0$.

2.2.2 Solution of the problem

In the problem above we have assumed that in the final system we can distinguish the particles of the first system from the other system. However we postulate that the particles are indistinguishable and each particle has a different state. That would change figure 2.2a to figure 2.2b.

Permutations of the same state:

- $N = 2$ there are 2 identical states.
- $N = 3$ there are 6 identical states.
- ...
- $N = N$ there are $N!$ identical states.

Therefore we must divide the number of states by $N!$ [4]. Now the number of configurations becomes

$$\Omega = V^N \left(\frac{U}{N} \right)^{\frac{3N}{2}} \frac{1}{N!}, \quad (2.44)$$

leading to entropy

$$S = Nk_B \left(\ln(V) + \frac{3}{2} \ln \left(\frac{U}{N} \right) \right) - k_B \ln(N!) \quad (2.45)$$

$$= Nk_B \left(\ln(V) - \ln(N) + \frac{3}{2} \ln \left(\frac{U}{N} \right) + 1 \right) \quad (2.46)$$

$$= Nk_B \left(\ln \left(\frac{V}{N} \right) + \frac{3}{2} \ln \left(\frac{U}{N} \right) + 1 \right). \quad (2.47)$$

Where we have used Stirling's approximation

$$\ln N! = \ln N - N. \quad (2.48)$$

The entropy of the total entropy before removal of the partition is $2S$ and after removal is now

$$S_{TOT} = 2Nk_B \left(\ln \left(\frac{2V}{2N} \right) + \frac{3}{2} \ln \left(\frac{2U}{2N} \right) + 1 \right). \quad (2.49)$$

so the difference between the final entropy and initial entropy is

$$\Delta S = S_{TOT} - 2S \quad (2.50)$$

$$= 2Nk_B \left(\ln(V) + \frac{3}{2} \ln \left(\frac{U}{N} \right) + 1 \right) - 2Nk_B \left(\ln \left(\frac{2V}{2N} \right) + \frac{3}{2} \ln \left(\frac{2U}{2N} \right) + 1 \right) \quad (2.51)$$

$$= 2Nk_B \left(\ln \left(\frac{V}{N} \right) - \ln \left(\frac{V}{N} \right) \right) = 0. \quad (2.52)$$

Which means a conservation of the total entropy over time of an isolated system, expressed as the second law of thermodynamics. With this example we see that the theory of indistinguishability should fit physical experimental data, not only in the quantum mechanical description, but also in the classical description.

2.3 Electromagnetic radiation

The two types of light that we discuss here are thermal light and coherent light. Coherent light and thermal light can be described by Fock states.

2.3.1 Thermal light

The random motion of a large number of particles inside a quantum system is called thermal motion and the electromagnetic radiation generated by this motion is called thermal radiation. This radiation is a spontaneous emission. Remembering from equation 2.7 that the energy of a photon in an electromagnetic mode is $E = h\omega$. The average number of photons [19] is given by

$$\langle N \rangle = \frac{1}{\exp \left(\frac{h\omega}{k_B T} \right) + \epsilon}, \quad (2.53)$$

where k_B is Boltzmann's constant and T the temperature. This results in three types of statistics.

- $\epsilon = -1$: *Bose-Einstein statistics*: for indistinguishable non-interactive bosons with quantum effects.

- $\epsilon = 0$: *Maxwell-Boltzmann statistics*: for distinguishable particles without quantum effects and for which there is no quantization in energy levels. Can be used for photons under certain conditions.
- $\epsilon = 1$: *Fermi-Dirac statistics*: for indistinguishable non-interactive fermions with quantum effects.

For high temperatures the ϵ term becomes too small and the photons that were originally described by Bose-Einstein statistics are described by the Maxwell-Boltzmann statistics.

To find the probability distribution for thermal photons described by Bose-Einstein statistics we start with the Boltzmann factor, from which we can calculate the probability to find n photons, at a certain temperature T : [28]

$$P_n = \frac{\exp\left(-\frac{E_n}{k_B T}\right)}{\sum_n \exp\left(-\frac{E_n}{k_B T}\right)}. \quad (2.54)$$

Since thermal photons are quantized as $E_n = n\hbar\omega$:

$$P_n = \frac{\exp\left(-\frac{n\hbar\omega}{k_B T}\right)}{\sum_n \exp\left(-\frac{n\hbar\omega}{k_B T}\right)} = \exp\left(-\frac{(n+1)\hbar\omega}{k_B T}\right) \left(\exp\left(\frac{\hbar\omega}{k_B T}\right) - 1\right). \quad (2.55)$$

Using the Bose-Einstein statistics for photons one finds

$$\langle n \rangle = \frac{1}{\exp\left(\frac{\hbar\omega}{k_B T}\right) - 1} \Rightarrow \exp\left(\frac{\hbar\omega}{k_B T}\right) = 1 + \frac{1}{\langle n \rangle} = \frac{\langle n \rangle + 1}{\langle n \rangle}. \quad (2.56)$$

Combining equation 2.55 and 2.56, one finds the following probability distribution for n thermal photons called the **Bose-Einstein distribution**.

$$P_n = \left(\frac{1}{\exp\left(\frac{\hbar\omega}{k_B T}\right)}\right)^{n+1} \left(\exp\left(\frac{\hbar\omega}{k_B T}\right) - 1\right) \quad (2.57)$$

$$= \left(\frac{\langle n \rangle}{\langle n \rangle + 1}\right)^{n+1} \frac{1}{\langle n \rangle} \quad (2.58)$$

$$= \frac{\langle n \rangle^n}{(\langle n \rangle + 1)^{n+1}}. \quad (2.59)$$

In figure 2.3 this equation is plotted for $\langle n \rangle = 5$.

2.3.2 Coherent light

Laser emission (above a certain threshold) consist of coherent light emission. As already mentioned we can describe coherent light by Fock states. In the basis of eigenstates $|\alpha\rangle$ of the annihilation operator the coherent states are defined as: [12, 13, 28, 36]

$$\hat{a}|\alpha\rangle = \alpha|\alpha\rangle. \quad (2.60)$$

In Fock states basis the eigenstates are written as

$$|\alpha\rangle = \exp\left(-\frac{|\alpha|^2}{2}\right) \sum_n \frac{\alpha^n}{\sqrt{n!}} |n\rangle. \quad (2.61)$$

To find the probability distribution for coherent photons we start with calculating the probability of finding a measurement result, described by equation 2.5. Using the description of coherent states in the Fock basis of equation 2.61 we find

$$P_n = |\langle n|\alpha\rangle|^2 \quad (2.62)$$

$$= \left| \exp\left(-\frac{|\alpha|^2}{2}\right) \frac{\alpha^n}{\sqrt{n!}} \right|^2 \quad (2.63)$$

$$= \exp\left(-|\alpha|^2\right) \frac{|\alpha|^{2n}}{n!}. \quad (2.64)$$

Which could be rewritten using the photon number operator of equation 2.21, $\hat{N} = \hat{a}^\dagger \hat{a}$, to the probability distribution for n coherent photons called the **Poisson distribution**

$$P_n = \exp(-\langle n \rangle) \frac{\langle n \rangle^n}{n!}, \quad (2.65)$$

where we used the relation between coherent states of equation 2.60 and the mean photon number

$$\langle n \rangle = \langle \alpha | \hat{N} | \alpha \rangle = \langle \alpha | \hat{a}^\dagger \hat{a} | \alpha \rangle = |\alpha|^2. \quad (2.66)$$

The comparison between the Bose-Einstein and Poisson distributions can be seen in figure 2.3. Note, that for large $\langle n \rangle$ the Poissonian distribution takes the shape of a Gaussian one, but for a single photon source the distribution is just a point in this graph with a probability of $P(1) \approx 1$.

2.4 Degree of indistinguishability

2.4.1 Description of single photons

Single photons can be described as wave packets in a pure quantum state, that produces a probability distribution for the outcome of each observable of the photon. Also,

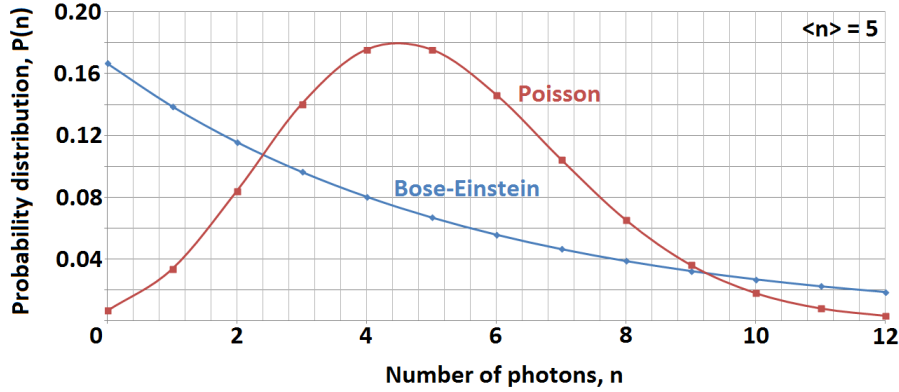


Figure 2.3: Graph displaying the different probability distributions $P(n)$ for Poisson and Bose-Einstein distribution for the expectation value $\langle n \rangle = 5$.

single photon quantum states are single excitations inside electromagnetic modes. The preparation of this state in Fock space is described as [37, 39]

$$|1\rangle = \int d\omega g(\omega) \hat{a}^\dagger(\omega) |0\rangle. \quad (2.67)$$

With the single photon creation operator acting on the vacuum state $|0\rangle$ in each mode of frequency ω . The initial occupation of the modes is defined by the normalized spectral probability amplitude function

$$\int_{-\infty}^{+\infty} d\omega |g_\omega(0)|^2 = 1. \quad (2.68)$$

This amplitude function varies for the shape of the photon, for example Gaussian shaped or sinc function shaped photons. The input state, in Fock space, for a single photon input is:

$$|1\rangle = \hat{a}^\dagger |0\rangle. \quad (2.69)$$

We can adapt this equation to contain more properties, for example a location r and a property of the single photon s :

$$|1\rangle_r = \hat{a}_s^\dagger |0\rangle_r. \quad (2.70)$$

To measure indistinguishability of single photons, **interferometry** experiments, allowing split up and combined electromagnetic waves resulting to interference, need to be done. In the case of two photons, in the quantum mechanical description, this is called two-photon interference. For splitting and combining a beam splitter is typically used, its classical and quantum-mechanical description is the subject of the next section.

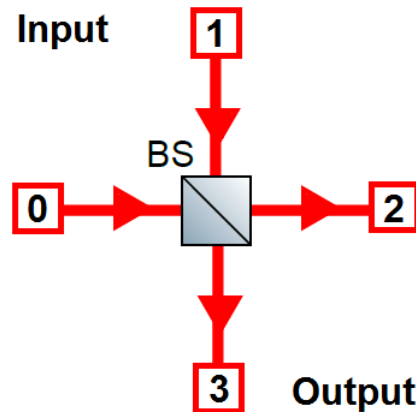


Figure 2.4: Beam splitter with input ports 0 and 1 and output ports 2 and 3.

2.4.2 Classical beam splitter

See figure 2.4 for a illustration of a beam splitter. The intensities of transmitted light $t_{\text{input, output}}$ and reflected light $r_{\text{input, output}}$ from input to output location is given by:

$$t_{02}, t_{13}, r_{03}, r_{12}. \quad (2.71)$$

Incident beams are E_0 and E_1 , so we can now write the transformation by the beam splitter as: [41]

$$E_2 = t_{02}E_0 + r_{12}E_1, \quad (2.72)$$

$$E_3 = r_{03}E_0 + t_{13}E_1, \quad (2.73)$$

$$\begin{bmatrix} E_2 \\ E_3 \end{bmatrix} = \begin{bmatrix} t_{02} & r_{12} \\ r_{03} & t_{13} \end{bmatrix} \begin{bmatrix} E_0 \\ E_1 \end{bmatrix}. \quad (2.74)$$

Where the matrix notation is to write the above equations collectively. For lossless beam splitters the sum of the intensities of the input and output beams should be the same due to energy conservation.

$$|E_2|^2 + |E_3|^2 = |E_0|^2 + |E_1|^2. \quad (2.75)$$

With equation 2.74 we can rewrite this:

$$\begin{aligned} & \left(|r_{12}|^2 + |t_{13}|^2 \right) |E_1|^2 + \left(|r_{03}|^2 + |t_{02}|^2 \right) |E_0|^2 \\ & + (r_{12}^* t_{02} + t_{02}^* r_{12}) (E_0 E_1) + (r_{03}^* t_{13} + t_{13}^* r_{03}) (E_0 E_1) \\ & = |E_0|^2 + |E_1|^2. \end{aligned} \quad (2.76)$$

Resulting in the following reciprocity relations: [12]

$$|r_{12}|^2 + |t_{13}|^2 = 1, \quad (2.77)$$

$$|r_{03}|^2 + |t_{02}|^2 = 1, \quad (2.78)$$

$$r_{12}^* t_{02} + t_{02}^* r_{12} = 0, \quad (2.79)$$

$$r_{03}^* t_{13} + t_{13}^* r_{03} = 0. \quad (2.80)$$

In general the following reciprocity relations are found based on energy conservation. For $|r_{12}| = |r_{03}|$ and $|t_{13}| = |t_{02}|$:

$$|r|^2 + |t|^2 = 1, \quad (2.81)$$

$$r^* t + t^* r = 0. \quad (2.82)$$

2.4.3 Quantum beam splitter

See figure 2.4 for a illustration of a lossless beam splitter. The intensities of transmitted light $t_{input,output}$ and reflected light $r_{input,output}$ from input to output location is given by equation 2.71. Incident beams are now replaced by annihilation operators \hat{a}_0 and \hat{a}_1 , so we can now write the transformation by the beam splitter as:

$$\hat{a}_2 = t_{02}\hat{a}_0 + r_{12}\hat{a}_1, \quad (2.83)$$

$$\hat{a}_3 = r_{03}\hat{a}_0 + t_{13}\hat{a}_1, \quad (2.84)$$

$$\begin{bmatrix} \hat{a}_2 \\ \hat{a}_3 \end{bmatrix} = \begin{bmatrix} t_{02} & r_{12} \\ r_{03} & t_{13} \end{bmatrix} \begin{bmatrix} \hat{a}_0 \\ \hat{a}_1 \end{bmatrix}. \quad (2.85)$$

For a **50:50 beam splitter**, reflectance and transmittance are equal, $|r|^2 = |t|^2 = \frac{1}{2}$, and because of the construction of the beam splitter there is a phase shift between the reflected and transmitted beam so we can choose:

$$t_{02} = t_{13} = \frac{1}{\sqrt{2}}, \quad (2.86)$$

$$r_{03} = r_{12} = \frac{i}{\sqrt{2}}. \quad (2.87)$$

This changes the transformation, and we can write the creation operators by taking the complex conjugate:

$$\hat{a}_2 = \frac{1}{\sqrt{2}} (\hat{a}_0 + i\hat{a}_1), \hat{a}_2^\dagger = \frac{1}{\sqrt{2}} (\hat{a}_0^\dagger - i\hat{a}_1^\dagger), \quad (2.88)$$

$$\hat{a}_3 = \frac{1}{\sqrt{2}} (i\hat{a}_0 + \hat{a}_1), \hat{a}_3^\dagger = \frac{1}{\sqrt{2}} (-i\hat{a}_0^\dagger + \hat{a}_1^\dagger). \quad (2.89)$$

If we rewrite this equations, we get the following **replacement rules**:

$$\hat{a}_1^\dagger = \frac{1}{\sqrt{2}} (i\hat{a}_2^\dagger + \hat{a}_3^\dagger), \hat{a}_0^\dagger = \frac{1}{\sqrt{2}} (\hat{a}_2^\dagger + i\hat{a}_3^\dagger). \quad (2.90)$$

This replacement rule can be used in the following notation:

$$|\text{Input}\rangle \rightarrow |\text{Output}\rangle. \quad (2.91)$$

The following example shows this notation for 1 photon input for the beam splitter.

Example: 1 photon input at the beam splitter

The input of the beam splitter is a single photon at port 1 and the vacuum state will transform from 0 and 1 to 2 and 3. We can write this, using equation 2.90, as:

$$\hat{a}_1^\dagger |0\rangle_0 |0\rangle_1 \rightarrow \frac{1}{\sqrt{2}} \left(i\hat{a}_2^\dagger + \hat{a}_3^\dagger \right) |0\rangle_2 |0\rangle_3, \quad (2.92)$$

or equivalently:

$$|0\rangle_0 |1\rangle_1 \rightarrow \frac{1}{\sqrt{2}} \left(i|1\rangle_2 |0\rangle_3 + |0\rangle_2 |1\rangle_3 \right). \quad (2.93)$$

This output state is an example of an **entangled state**. This state cannot be described by only describing one output port. The result shows that one of the output port will be in vacuum when the other has a single photon incident.

2.4.4 Two-photon interference, polarization degree of freedom

We are now ready to describe the indistinguishability of single photons. Photons can be (in)distinguishable in several degrees of freedom, we focus here on polarization. We start with the same definitions for the beam splitter on figure 2.4 from the previous section. Now 1 photon is at port 0 and the other photon is at port 1 having orthogonal polarization if the photons are **distinguishable**. If we replace the \hat{a}^\dagger operator by the single-photon polarization operator (horizontal or vertical) this will result in the following output state:

$$\begin{aligned} \hat{H}_0^\dagger \hat{V}_1^\dagger |0\rangle_0 |0\rangle_1 &\rightarrow \frac{1}{2} \left(\hat{H}_2^\dagger + i\hat{H}_3^\dagger \right) \left(i\hat{V}_2^\dagger + \hat{V}_3^\dagger \right) |0\rangle_2 |0\rangle_3 \\ &= \frac{1}{2} \left(i\hat{H}_2^\dagger \hat{V}_2^\dagger + \hat{H}_2^\dagger \hat{V}_3^\dagger - \hat{H}_3^\dagger \hat{V}_2^\dagger + i\hat{H}_3^\dagger \hat{V}_3^\dagger \right) |0\rangle_2 |0\rangle_3. \end{aligned} \quad (2.94)$$

Where we have used the replacement rules of equation 2.90. The output state can be written also in the Fock basis with probability $P = \frac{1}{4} + \frac{1}{4} = \frac{1}{2}$ to find two photons at one output port and the same probability to find only one at each of the output ports.

Now for **indistinguishable photons** they have parallel polarizatton. We know from equation 2.31 that identical bosons, and thus indistinguishable photons, commute with each other:

$$[\hat{H}_i^\dagger, \hat{H}_j^\dagger] = \hat{H}_i^\dagger \hat{H}_j^\dagger - \hat{H}_j^\dagger \hat{H}_i^\dagger = 0. \quad (2.95)$$

Resulting in the following output state:

$$\hat{H}_0^\dagger \hat{H}_1^\dagger |0\rangle_0 |0\rangle_1 \rightarrow \frac{1}{2} \left(\hat{H}_2^\dagger + i\hat{H}_3^\dagger \right) \left(i\hat{H}_2^\dagger + \hat{H}_3^\dagger \right) |0\rangle_2 |0\rangle_3 \quad (2.96)$$

$$= \frac{1}{2} \left(i\hat{H}_2^\dagger \hat{H}_2^\dagger + \hat{H}_2^\dagger \hat{H}_3^\dagger - \hat{H}_3^\dagger \hat{H}_2^\dagger + i\hat{H}_3^\dagger \hat{H}_3^\dagger \right) |0\rangle_2 |0\rangle_3 \quad (2.97)$$

$$= \frac{1}{2} \left(i\hat{H}_2^\dagger \hat{H}_2^\dagger + i\hat{H}_3^\dagger \hat{H}_3^\dagger \right) |0\rangle_2 |0\rangle_3 \quad (2.98)$$

$$= \frac{1}{\sqrt{2}} (|2_H\rangle_2 |0\rangle_3 - |0\rangle_2 |2_H\rangle_3). \quad (2.99)$$

Where in the last step we used equation 2.17 to get the $\sqrt{2}$ in the output state. Now the probability to find the two photons not at the same output port, the coincidence probability, is $P = 0$! So we get a photon bunching effect which is called the **Hong-Ou-Mandel effect** [15]. The full description of this effect:

Hong-Ou-Mandel effect

The Hong-Ou-Mandel (HOM) effect is an effect between two indistinguishable single photons if they enter, for example, a beam splitter at different ports. They have to be identical in all degrees of freedom (polarization, spatial, temporal etc.) for this quantum interference effect to happen.

If two indistinguishable single photons enter at different ports, the following two cases get cancelled out due to destructive interference:

- The photons are reflected.
- The photons are transmitted.

In conclusion: due to the HOM effect both photons will exit the beamsplitter at the same port.

2.4.5 Two-photon interference, temporal degree of freedom

For a photon with a spectral amplitude function we can describe the temporal degrees of freedom between the photons. The temporal wavefunction overlap is needed to describe the distinguishability. This overlap is shown in figure 2.5. In this thesis is described how to detect distinguishability with experiments in the spatial degrees of freedom. Here we study in more detail the photon spectrum [5]. Since we now have two different spectral amplitude functions for the single photons, A and B , we can describe the quantum states using equation 2.67 and the beam splitter ports from figure 2.4,

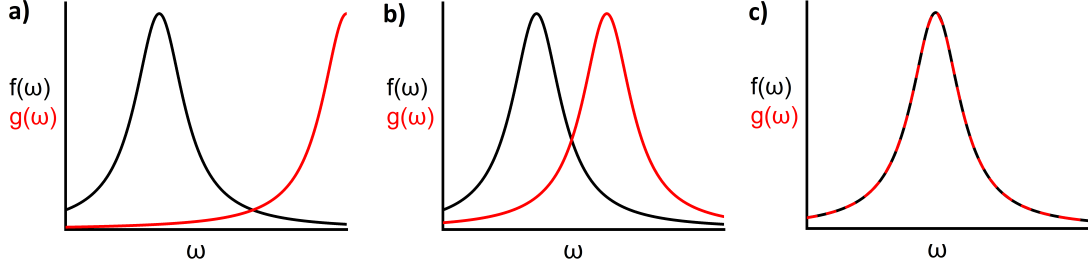


Figure 2.5: Spectral wave function overlap between two spectral amplitude functions for two photons. a) Almost no overlap, b) partial overlap, c) fully overlap so indistinguishable photons.

where we have introduced a **time delay** τ for one of the photons:

$$|1\rangle_0 = \int d\omega_1 f(\omega_1) \hat{A}^\dagger(\omega_1) |0\rangle_0, \quad (2.100)$$

$$|1\rangle_1 = \int d\omega_2 g(\omega_2) \hat{B}^\dagger(\omega_2) \exp(-i\omega_2\tau) |0\rangle_1. \quad (2.101)$$

The total two-photon input state then is:

$$|1\rangle_0 |1\rangle_1 = \int d\omega_1 f(\omega_1) \hat{A}^\dagger(\omega_1) \int d\omega_2 g(\omega_2) \hat{B}^\dagger(\omega_2) \exp(-i\omega_2\tau) |0\rangle_0 |0\rangle_1. \quad (2.102)$$

The total two-photon output state, using the replacement rules of equation 2.90, then is:

$$|\Psi_{Out}\rangle = \int d\omega_1 f(\omega_1) \int d\omega_2 g(\omega_2) \exp(-i\omega_2\tau) \quad (2.103)$$

$$\times \left(i\hat{A}^\dagger(\omega_1) + \hat{B}^\dagger(\omega_1) \right) \left(\hat{A}^\dagger(\omega_2) + i\hat{B}^\dagger(\omega_2) \right) |0\rangle_2 |0\rangle_3. \quad (2.104)$$

With a lot of algebra, see [5], we can find the **coincidence probability** (cc), which is the detection of one photon in each output. If the photons are completely indistinguishable and the wave functions overlap fully, this probability is zero due to the Hong-Ou-Mandel effect. For two arbitrary spectral amplitude functions this becomes:

$$P_{cc} = \frac{1}{2} - \frac{1}{2} \int d\omega_1 f^*(\omega_1) g(\omega_1) \exp(-i\omega_1\tau) \int d\omega_2 g^*(\omega_2) f(\omega_2) \exp(i\omega_2\tau). \quad (2.105)$$

When the wave functions overlap, $f(\omega_i) = g(\omega_i)$, this becomes:

$$P_{cc} = \frac{1}{2} - \frac{1}{2} \int d\omega_1 |f(\omega_1)|^2 \exp(-i\omega_1\tau) \int d\omega_2 |f(\omega_2)|^2 \exp(i\omega_2\tau). \quad (2.106)$$

With this probability we are able to calculate photon distinguishability. In general, for the Hong-Ou-Mandel experiment, the coincidence probability of two independent photons is given by their mean magnitude-squared overlap M [37]

$$P_{cc} = \frac{1}{2} (1 - M). \quad (2.107)$$

Also the spatial degrees of freedom can be used to tune the distinguishability, in particular important here is the spatial overlap between the light beams in our setup. If the setup is partially misaligned, the Hong-Ou-Mandel quantum interference effect, described in the last section, will only partially take place.

Experimental setup

The ComponentLibrary by Alexander Franzen is used for the generation of pictures of optical setups and schemes in this thesis.

In this chapter we describe the optical setup that was built for the experimental construction of multi photon entanglement. Omitted in this chapter is the **Quantum Dot setup** which we use to generate the single photon stream. Quantum dots placed inside a cavity can produce deterministically single photons, instead of a probabilistically source with Spontaneous Parametric Down-Conversion (SPDC). The scheme which we will be using is an adaptation of the deterministic scheme of Y. Pilnyak et al. (2017) [30]. This scheme is based on transforming a sequence of single photons (for details about our quantum-dot based single photon source, see Ref. [34]) into a linear cluster state entangled in the polarization degree of freedom. Photons, existing in a quantum superposition of polarization states, can be seen as qubits (two-level quantum systems). Measurements on single-qubits in photonic cluster states can be used for quantum computational tasks [6, 20, 21].

3.1 Contents of the optical setup

In this thesis we build this experimental setup, which has the following parts:

- **Hanbury Brown and Twiss (HBT) detection setup.** See section 4.3.
- **“No loop” setup** where the loop is blocked. See section 5.1.
- **Delay loop setup** where photons can make maximally one loop. See section 5.2.
- **Open loop** with a half-wave plate in it used for the **creation of cluster states.** See section 6.2.

The main optical components of our optical setup are presented in figure 3.1. A description of several components:

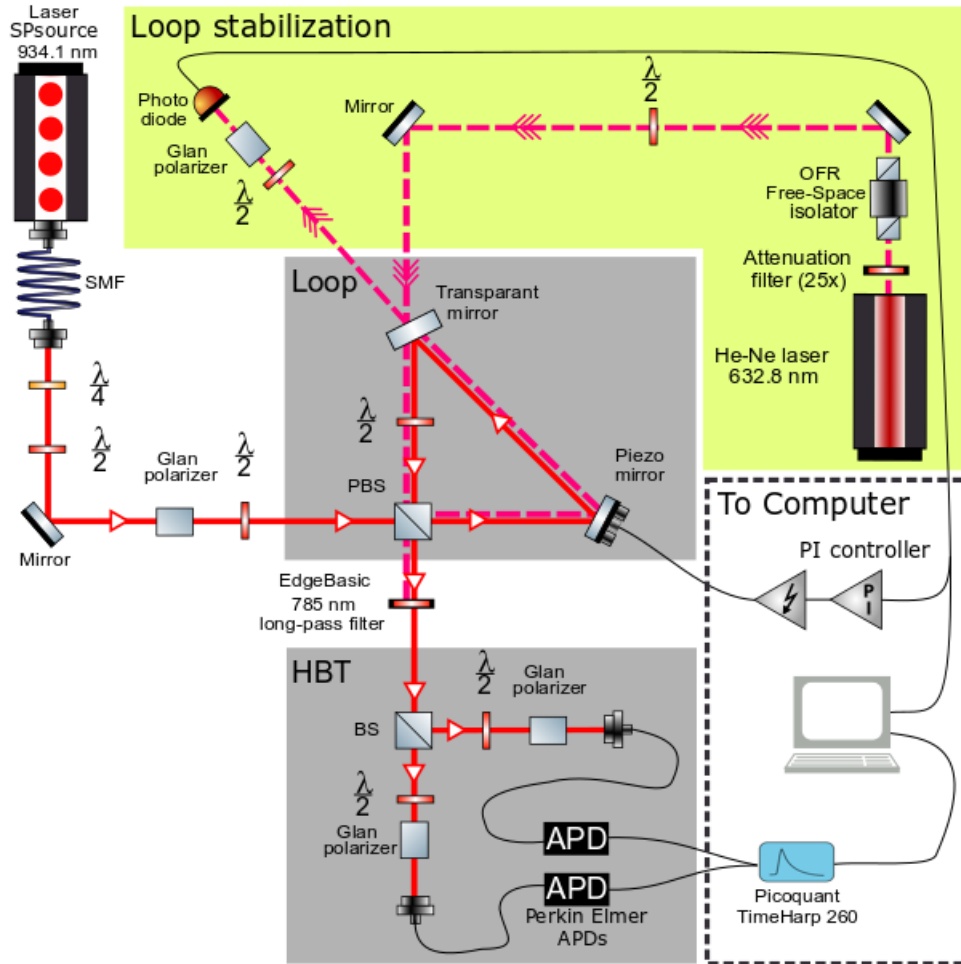


Figure 3.1: Optical setup used in this thesis for the generation of cluster states based on a single photon (SP) source. Arrows in the figure illustrate the direction of the photons and light beams. The SP light passes through a single mode fiber (SMF), through wave plates, polarizers, (polarizing) beam splitters (BS), a Loop and the Perkin Elmer Avalanche Photon Detectors (APD) in the Hanbury Brown & Twiss (HBT) setup. The loop stabilization is done with an attenuated He-Ne laser, that is sent through an optical isolator, before it enters the loop. Data is processed by a computer, which also controls the piezo mirror in the loop with a proportional-integral controller.

- **Tunable laser** (Velocity, model 6319, 930-945 nm from New Focus [1]) most of the time operating around 934.1 nm; used for quantum dot excitation.
- **He-Ne laser** that operates at 632.8 nm used to stabilize the loop.
- **Quarter-wave** $\left(\frac{\lambda}{4}\right)$ **plate** which can be used for the conversion between linearly and circularly polarized light. The combination of the $\frac{\lambda}{4}$ wave plate and $\frac{\lambda}{2}$ plate is used in combination with a polarizer to optimize the incoming photon rate.
- **Half-wave** $\left(\frac{\lambda}{2}\right)$ **plate** rotates the plane of polarization from the light source to any other plane that is desired.
- **Glan Polarizer** (Glan-Laser Calcite Polarizers from Thorlabs) used to pass polarized light in a specific orientation and block other polarizations.
- **Beam splitter** (BS).
- **Polarizing beam splitter** (PBS) transmits H-polarization and reflects V-polarization, note that the reflected light contains a small admixture of H-polarization.
- **Optical isolator** (OFR Free-Space Isolator) used to protect the He-Ne laser source from back reflected light from the loop.
- **Filters**. The filter after the loop (785 nm long-pass filter from EdgeBasic) passes most of the light above 785 nm and transmits the least light at around 630 nm.
- **Photo diode** (SI Amplified Detector PDA100A by Thorlabs).
- **Avalanche Photon Detectors** (Perkin Elmer APDs) used to detect single photons, the dead time of the detectors is 60 ns.
- **PI controller** used for the feedback mechanism for the stabilization of the loop.
- **TimeHarp** (Picoquant TimeHarp 260) is the card which records the correlations between the detected photons.

Other software we used are LabView and Spiricon beam profiler software. In the next section we will discuss the result of different polarizations in this setup.

3.2 Polarization in the optical setup

Light first goes through a \hat{H}^+ -polarizer as can be seen in figure 3.2. Next the polarized light becomes diagonally polarized by a $\frac{\lambda}{2}$ -wave plate. To change the polarization by 45° one must rotate the wave plate by 22.5° . This effect is as follows:

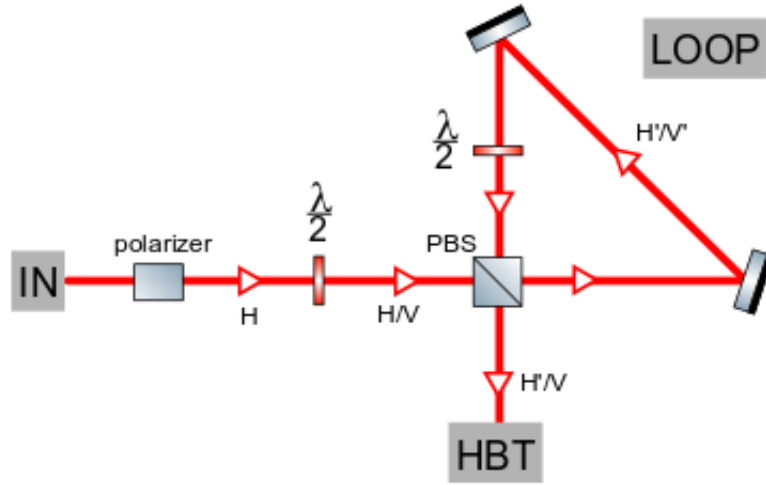


Figure 3.2: Block diagram of the polarizing beam splitter (PBS) part. Incoming polarized light from the single photon source can enter the loop or go to the Hanbury Brown and Twiss (HBT) detection setup through the PBS. Subsequently incoming polarized light from the loop can continue in the loop or go to the HBT setup through the PBS. Single photons with an apostrophe for a certain polarization went through the loop.

$$\hat{H}^+ \xrightarrow{45^\circ} \frac{1}{\sqrt{2}} (\hat{H}^+ + \hat{V}^+) \quad (3.1)$$

$$\hat{V}^+ \xrightarrow{45^\circ} \frac{1}{\sqrt{2}} (\hat{H}^+ - \hat{V}^+). \quad (3.2)$$

The superposition of an equal amount of horizontally and vertically polarized light enters the PBS. Horizontally polarized light gets transmitted and vertically polarized light gets reflected as can be seen in the figure. Light from the loop, see figure 3.2, becomes again diagonally polarized by a $\frac{\lambda}{2}$ -wave plate and again the PBS reflects \hat{V}^+ -polarized light and transmits \hat{H}^+ -polarized light. We can in principle make all rotations, for example the diagonal basis, with a $\frac{\lambda}{2}$ -wave plate, but not the change from the (H,V)-basis to a (L,R) circular basis. This can be done by the $\frac{\lambda}{4}$ -wave plate.

Photon interference and bunching

In this chapter we discuss and measure the visibility before we perform an interferometric measurement. This measurement uses the Hanbury Brown and Twiss effect, which we test for the single photon source solely by our detectors. Correlations are introduced and light can be bunched, antibunched or coherent. Finally beamprofiles are taken to test the alignment and a normalization fit function is introduced.

4.1 Interference visibility

To measure the coherence, meaning all correlation properties, of two waves we can use the definition of the interferometric visibility given by: [24]

$$V = \frac{\langle I \rangle_{max} - \langle I \rangle_{min}}{\langle I \rangle_{max} + \langle I \rangle_{min}}. \quad (4.1)$$

Here $\langle I \rangle_{max}$ and $\langle I \rangle_{min}$ are given by: [12]

$$\langle I \rangle_{max} = I_1 + I_2 + 2\sqrt{I_1 I_2} |\gamma^{(1)}| \quad (4.2)$$

$$\langle I \rangle_{min} = I_1 + I_2 - 2\sqrt{I_1 I_2} |\gamma^{(1)}|. \quad (4.3)$$

Where $|\gamma^{(1)}|$ is the first-order **classical** coherence function and I_1 and I_2 are the intensities of the first and second light field. First order coherence depends on the interference of electromagnetic fields, second order coherence depends on correlations between intensities of these fields and there are also higher orders of coherence. The **quantum** first order coherence function $|g^{(1)}|$ can be constructed in the same way, so:

- $|\gamma^{(1)}| = |g^{(1)}| = 1$: Complete coherence
- $|\gamma^{(1)}| = |g^{(1)}| = 0$: Incoherence
- $1 > |\gamma^{(1)}| > 0$ and $1 > |g^{(1)}| > 0$: Partial coherence

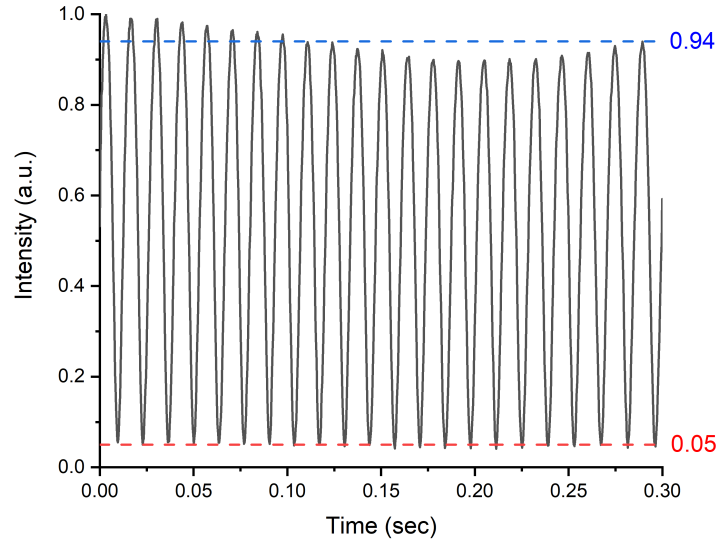


Figure 4.1: Visibility measurement in our setup. The intensity in arbitrary units is measured as a function of time.

4.1.1 Example: measurement of the visibility

In figure 4.1 a visibility measurement is shown we did during our setup alignment. This can only be done with an open loop without a half-wave plate inside the loop. In order to align the setup we would like to improve the visibility to a level above 90%, after subtraction of the background noise of the photo diode. For this measurement we got the following values for the intensities: $\langle I \rangle_{max} = 0.94$ and $\langle I \rangle_{min} = 0.05$ in a scanning time of 0.3 sec, resulting in:

$$V = \frac{0.94 - 0.05}{0.94 + 0.05} = \frac{0.89}{0.99} \approx 90\%. \quad (4.4)$$

This is a quantification of the coherence between the two fields in the setup. For a second order coherence function we must look at a correlation effect in intensities between the fields which can be done by the Hanbury Brown and Twiss effect described in the next section.

4.2 Hanbury Brown and Twiss effect

The description of fluctuations of intensity in a light beam is done by performing an Hanbury Brown and Twiss (1956) experiment [14]. Experimentally we need for this a 50/50 beamsplitter and the Picoquant TimeHarp 260 card. This card records the time differences between detected photons. As can be seen in figure 4.2 the combination of

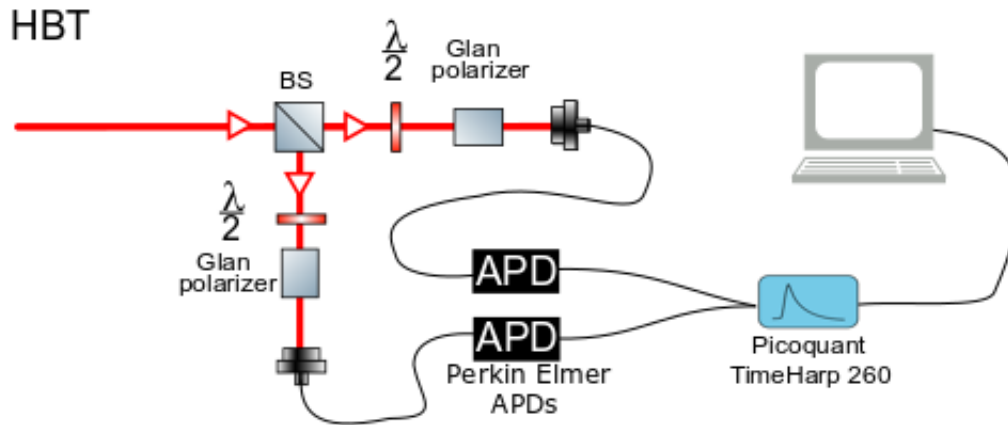


Figure 4.2: Optical setup for measuring the Hanbury Brown and Twiss effect(s).

$\frac{\lambda}{2}$ -wave plate and polarizer can be used to rotate the polarization of the light in any direction we want.

Generally, light is categorized according to its correlations:

- **Bunched** (chaotic) light: Photons tend to cluster together.
- **Antibunched** light: Light produced by a single photon source where never two photons are detected at the same time.
- **Coherent** (random) light: Time difference between the photons is random, for example for continuous wave laser light.

The measure for the classical and quantum mechanical second-order coherence, or in our case the autocorrelation of a light beam, is given by: [10]

$$g_{class}^{(2)}(\tau) = \frac{\langle I(t)I(t+\tau) \rangle}{\langle I(t) \rangle \times \langle I(t+\tau) \rangle} \quad (4.5)$$

$$g^{(2)}(\tau) = \frac{\langle N_1(t)N_2(t+\tau) \rangle}{\langle N_1(t) \rangle \times \langle N_2(t+\tau) \rangle}. \quad (4.6)$$

Where the intensities or photon detection of the light at time t and at time $t + \tau$ are considered. With the use of normal ordering, we get the creation and annihilation operator notation for the second order correlation function:

$$g^{(2)}(\tau) = \frac{\langle \hat{a}_1^\dagger(t)\hat{a}_2^\dagger(t+\tau)\hat{a}_2(t+\tau)\hat{a}_1(t) \rangle}{\langle \hat{a}_1^\dagger(t)\hat{a}_1(t) \rangle \langle \hat{a}_2^\dagger(t+\tau)\hat{a}_2(t+\tau) \rangle}. \quad (4.7)$$

The properties of $g^{(2)}(\tau)$ are:

- **Bunched** chaotic light: $g^{(2)}(0) > 1$.
- **Antibunched** light: $g^{(2)}(0) < 1$.
- **Coherent** (random) light: $g^{(2)}(0) = 1$.

Under the assumption $g^{(2)}(\tau) = 1$ for $|\tau| \gg 0$

This function is simpler for $\tau = 0$, which is useful to measure the single photon purity with our HBT setup. Therefore with a little bit of algebra, using equations 2.17 and 2.19, we can now write for the photon number operator N :

$$g^{(2)}(0) = \frac{\langle N(N-1) \rangle}{\langle N \rangle^2}. \quad (4.8)$$

For the number state input $|n\rangle$ we get:

$$g^{(2)}(0) = \frac{\langle n|N(N-1)|n\rangle}{\langle n|N^2|n\rangle} = \frac{n(n-1)}{n^2} = \frac{n-1}{n}. \quad (4.9)$$

Which is 0 for $n = 0$ or 1.

4.3 Hanbury Brown and Twiss experiment

For this experiment we couple light from the quantum dot setup into an optical fiber containing a beam splitter. A scheme for the HBT setup can be seen in figure 4.3. See the table for all the properties.

Single photon purity. Remembering that antibunched light gives $g^{(2)}(0) < 1$, we can determine the "purity" of the single photon source experimentally as the visibility of the HOM dip in a $g^{(2)}$ -measurement. However this renders a discouraging estimation of the purity, because of the detector response. We have to take the convolution between the theoretical $g^{(2)}$ and instrumental response function, $g_{theory}^{(2)} \otimes IRF$, to find the real value. The limitation of the single photon measurements of $g^{(2)}$, excited by a CW (continuous wave) laser, is by detector jitter. The degree of indistinguishability between quantum states is also indicated by this dip and we want to characterize the single photon degree of purity only. This can be done by the width of the HOM dip and the spectrum of the photon, as is shown by K. N. Cassemiro et al. (2010) [7]. If the photons are completely indistinguishable the M from equation 2.107 is equal to the HOM visibility. So the purity of single **indistinguishable** photons is:

$$\text{Purity} = 1 - g^{(2)}(0) \quad (4.10)$$

Duration	188 sec
#coincidences($\tau \gg 0$)	275
Normalization	$\frac{\#coincidences}{275}$

Table 4.1: Table containing the properties of the HBT experiment.

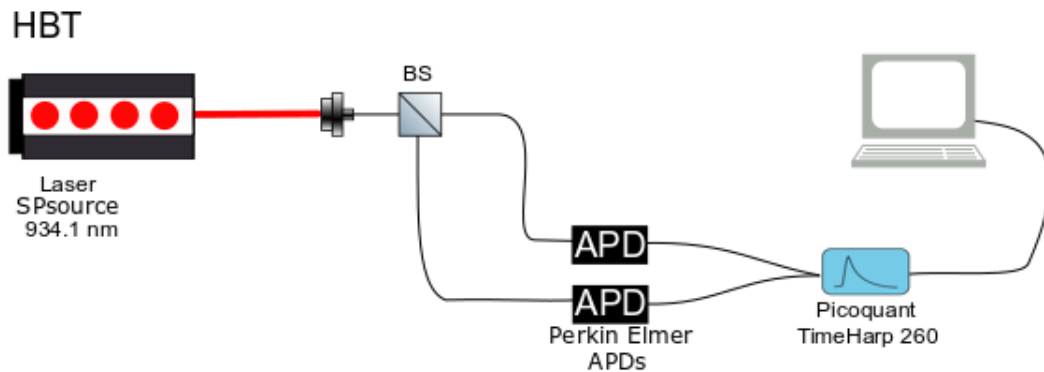


Figure 4.3: Scheme of the HBT setup for the HBT experiment with only the Quantum Dot single photon source.

Conclusion. We first normalize the graph and next we plot the $g^{(2)}$ in figure 4.4. The number of coincidences is low since we measure only for 188 sec, but we can clearly see the dip in the graph at $g^{(2)}(0)$. The fit through our data in this normalized graph is a Lorentzian function given by the following formula:

$$g_{Lorentzian}^{(2)}(\tau) = 1 - \frac{0.6}{16\tau^2 + 1}, \quad (4.11)$$

with τ the time delay between detections in ns. We see that our normalization results in a dip $g^{(2)}(0) \approx 0.4$, which results in a purity of 60%. In theory a purity of close to 100% can be reached. In the following sections we would like to characterize the alignment of our setup and the normalization fit we use in this thesis.

4.4 Alignment of the setup

The beam profile of the separated laser beams, from the same source, and the slightly misaligned beams can be seen in figure 4.5. The misalignment of the loop will still cause (partial) quantum interference, however the separated beams do not interfere at all. Aligning the setup would thus mean that at every point in the setup the beams overlap.

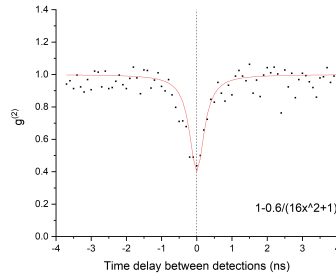


Figure 4.4: Measurement of the HBT setup experiment. This is a normalized $g^{(2)}$ graph with a Lorentzian fit through the data points.

Also when we mention the polarization configuration in later chapters, the first letter is the polarization of detector A and the second letter is the polarization of detector B. Before each experiment we align (or misalign) the setup, measure the visibilities of both detectors, calibrate the waveplates in front of the detectors and measure the coupling of the light into the optical fiber to the detectors. After each experiment we measure again the visibilities of both detectors.

4.5 Normalization fit

Since we measure at high laser power, to increase the number of coincidences, our second order correlation measurements are difficult to normalize. Higher laser power results in an overall bunching peak, which is visible in figure 4.6. This is most likely caused by spectral diffusion of background charges due to the strong laser drive. See table 4.2 for the parameters. We could measure at lower powers, but this would increase the measurement time. In future experiments this is the idea, however for the data that we obtained to write this thesis this was not implemented. Therefore we try to removing the overall bunching with a fitting formula. First we normalize the graphs by dividing the number of coincidences by the value for $\tau \gg 0$. Next we remove the bunching by dividing the number of coincidences by the following fit functions:

- **Without loop** - Bunching fit, see figure 4.6a:

$$g^{(2)}(\tau) = A \exp(-\lambda |\tau - \tau_0|) + 1. \quad (4.12)$$

- **With loop** - Bunching fit, see figure 4.6b.

$$g^{(2)}(\tau) = A \exp\left(-\frac{|\tau - \tau_0|^2}{2\sigma^2}\right) \times \exp(-\lambda |\tau - \tau_0|) + 1. \quad (4.13)$$

Where τ_0 is the measured time delay of the detectors and optical fibers with the VV configuration, in order to determine the point in time when $\tau = 0$. A is the height of the

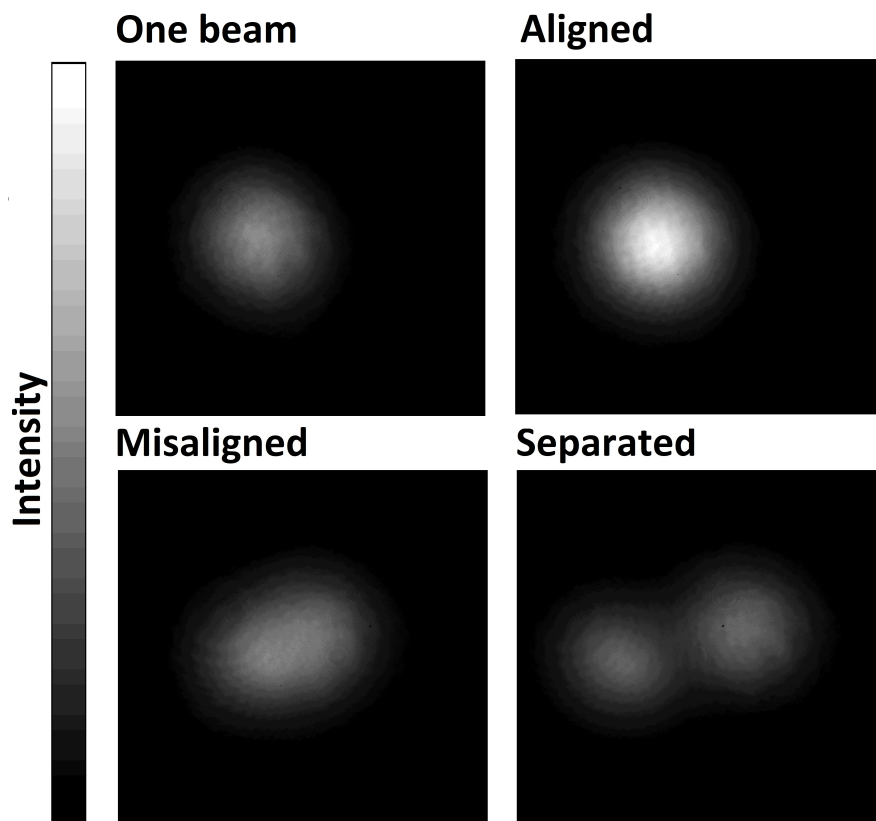


Figure 4.5: Beam profiles, taken directly after the loop of the optical setup, for a) one beam if the loop is blocked ("No loop"), b) aligned beams if the light from the loop and the light not going into the loop overlaps, c) misaligned beams and d) separated beams. The greyscale indicates the intensities of the laser light.

overall bunching in comparison to $g^{(2)}(\tau) = 1$. λ and σ are fit parameters, which should be studied in future research. Adding a loop to the setup will change this function, see table 4.2 below:

Detector A,B	VV ("No loop")	HH (Delay loop)
Duration	50 min	50 min
#coincidences($\tau \gg 0$)	11148	9700
Det. A visibility	95%	96%
Det. B visibility	90%	92%
Normalization	$\frac{\#coincidences}{11148}$	$\frac{\#coincidences}{9700}$
Parameters $\tau_0, A,$	-0.43, 0.28	-0.64, 0.11
Parameters σ, λ	$\infty, 0.21$	17.09, 0.11
$g^{(2)}(0)$	0.70	0.95
$g^{(2)}(-3.5), g^{(2)}(3.5)$	0.97, 0.99	0.89, 0.89

Table 4.2: Table containing the properties of the HH and VV configuration for the normalization fit cluster state setup experiment 2. See figure 4.6a and b.

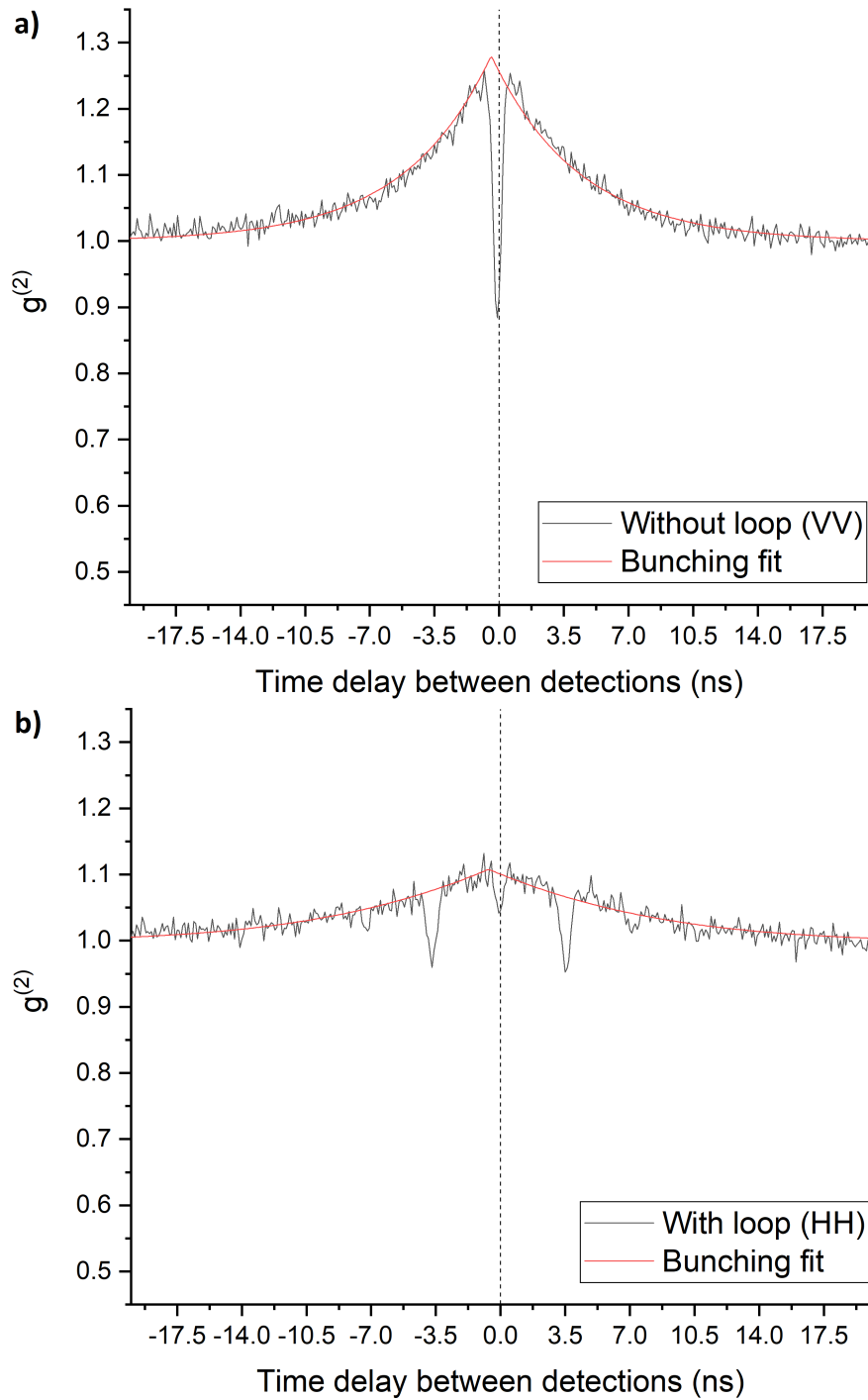


Figure 4.6: Second-order correlation measurements with and without loop. The fits from the bunching formulas are also plotted. a) $g^{(2)}$ without loop for a VV measurement. b) $g^{(2)}$ with loop for a HH measurement. See table 4.2.

Spatial alignment

In this chapter we investigate the Hanbury Brown and Twiss effect through our setup and create predictions. A specially designed loop setup is used for the generation of cluster states, but here we first examine the setup without a loop, the "No loop" setup and next we look at a Delay loop setup with one round trip R.

5.1 "No loop" setup

The single photon source we use in our setup produces single photons with a high purity, see section 4.3 for the experimental result of only the HBT effect for the two detectors. In this section we investigate the HBT effect in our "No loop" setup. The scheme of this setup is given in figure 5.1. The first letter and second letter of the polarization configuration are the detected polarizations of detector A and B.

5.1.1 "No loop" prediction

The prediction is based on a stream of photons from quantum dot excitation by a continuous wave laser (CW). Results are described in creation operator notation acting on vacuum state. We assume that the photons are perfectly indistinguishable.

Single photon input

Here \hat{P}_t^\dagger is the quantum state creation operator, with time t and polarization P , acting on $|Vac\rangle$. For the $\frac{\lambda}{2}$ -wave plate we use equations 3.1 and 3.2.

After the $\frac{\lambda}{4}$ -wave plate and $\frac{\lambda}{2}$ -wave plate, incoming light gets horizontally polarized by the polarizer. The effect of the next optical elements is as follows:

$$\hat{H}_t^\dagger \xrightarrow{\text{WP}} \frac{1}{\sqrt{2}}(\hat{H}_t^\dagger + \hat{V}_t^\dagger) \xrightarrow{\text{PBS}} \hat{V}_t^\dagger. \quad (5.1)$$

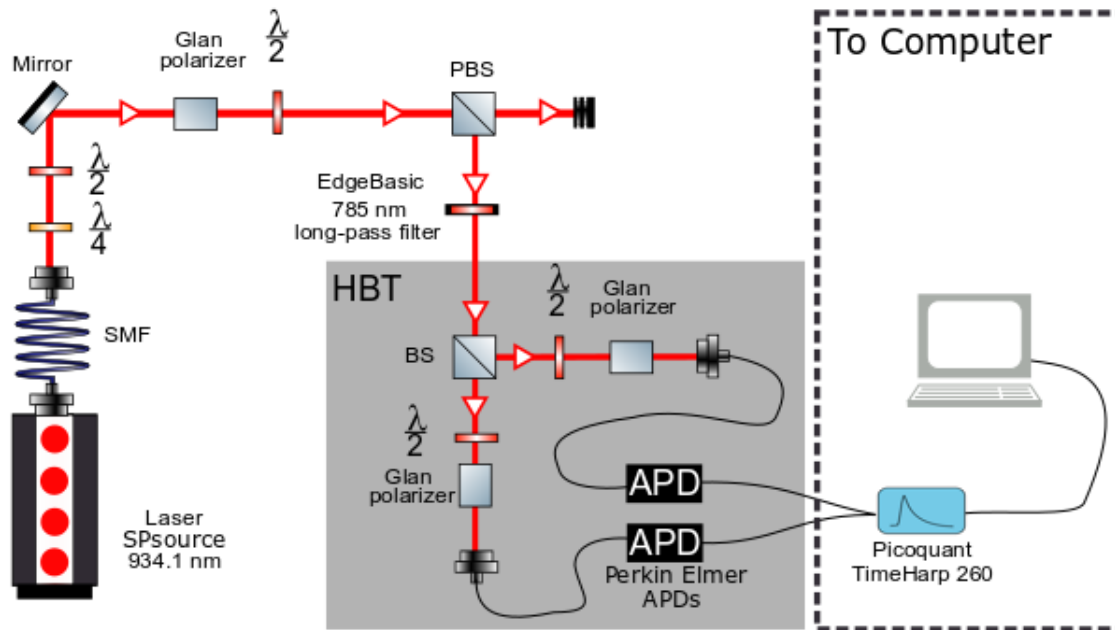


Figure 5.1: Scheme of the HBT setup for the “No loop” experiment with the quantum dot single photon source light entering various optical elements.

Where transmitted light, horizontally polarized, after the PBS enters an optical beam dump used to absorb beams for lab safety and to block the light from entering the loop.

Predictions

- Single photons reaching the detector are vertically polarized.
- No coincidences possible between horizontally and vertically polarized photons, since horizontally polarized photons reach a beam dump.
- Only a VV experiment, where both detectors are set to V polarization, will result in a single photon dip. Which is the HOM dip that shows the single photon purity. HV, VH and HH experiments will not result in coincidence counts, because all photons are vertically polarized.

5.1.2 “No loop” experiment

For this experiment we block the loop in the setup to test the prediction. A scheme for the setup can be seen in figure 5.1. See table 5.1 for all the properties of the VV, HV, VH and HH configuration measurements.

In figure 5.2 we can see the results of our experiment for the VV and HH configuration. The normalized VV configuration is plotted in figure 5.3. The HV, VH configurations from table 5.1 are not plotted since the amount of coincidence counts is many times more for the VV configuration.

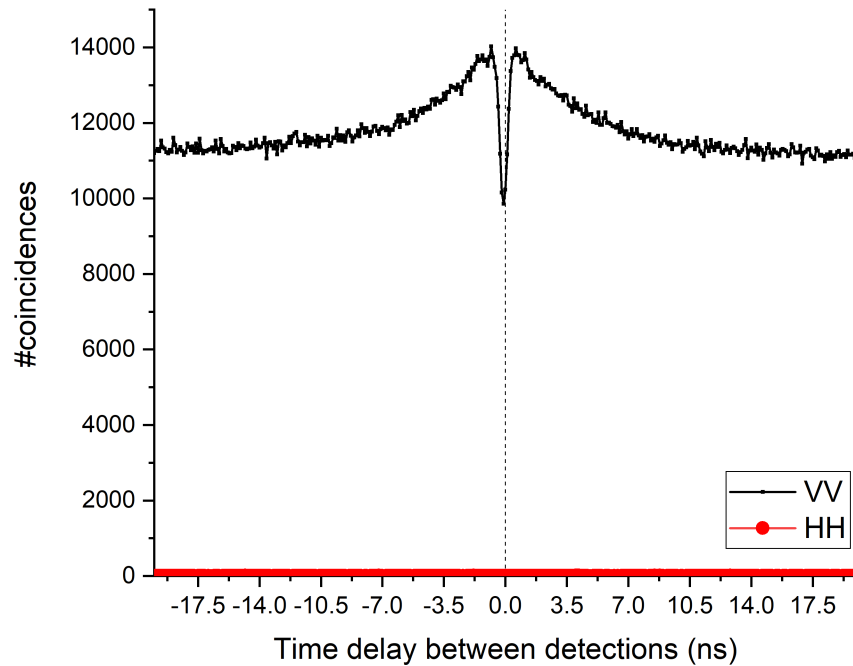


Figure 5.2: Coincidences vs the time delay between detections for HH and VV configuration in the "No loop" setup experiment. HH overlaps the x-axis in this graph. HV and VH configurations are not plotted. See table 5.1.

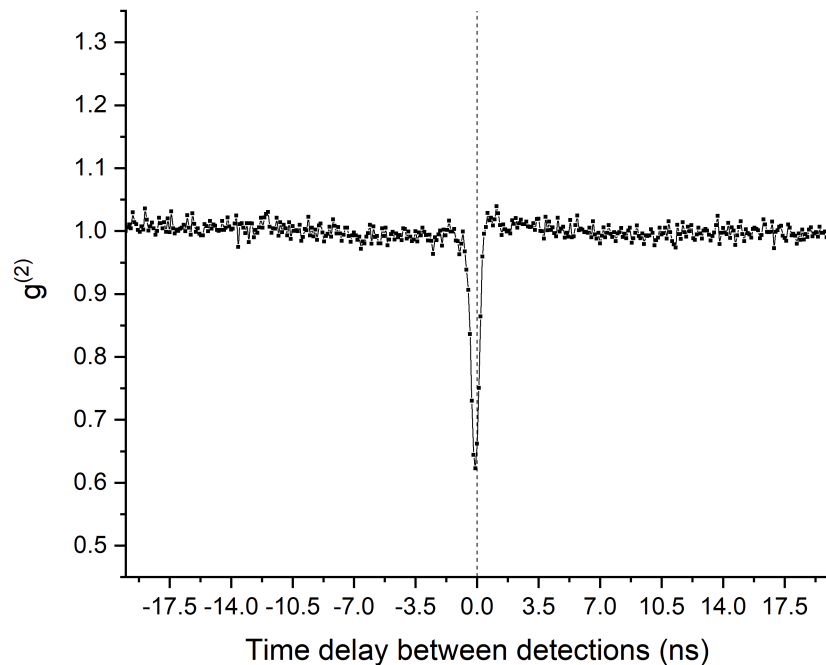


Figure 5.3: $g^{(2)}$ vs the time delay between detections for the VV configuration in the "No loop" setup experiment. See table 5.1.

Detector A,B	HH	HV	VH	VV
Duration	60 min	60 min	60 min	60 min
#coincidences($\tau \gg 0$)	5	126	382	11148
SP counts (at A)	2e3	2e3	1.8e5	1.8e5
Det. A visibility	90%	90%	90%	90%
Det. B visibility	86%	86%	86%	86%
Normalization	$\frac{\#coincidences}{5}$	$\frac{\#coincidences}{126}$	$\frac{\#coincidences}{382}$	$\frac{\#coincidences}{11148}$
Parameters $\tau_0, A,$	-, -	-0.33, 0.20	-0.33, 0.25	-0.43, 0.28
Parameters σ, λ	-, -	$\infty, 0.20$	45.25, 0.19	$\infty, 0.21$
$g^{(2)}(0)$	1.00	0.70	0.67	0.70
$g^{(2)}(-3.5), g^{(2)}(3.5)$	1.00, 1.00	0.91, 0.85	0.95, 0.89	0.97, 0.99

Table 5.1: Table containing the properties of HH, HV, VH and VV configuration for the “No loop” setup experiment. See figure 5.2 and 5.3.

Conclusions

- Single photons reaching the detector are indeed vertically polarized, as predicted.
- Almost no coincidences possible between horizontally and vertically polarized photons, since horizontally polarized photons reach a beam dump. The detected coincidences are probably because of the inaccuracy of the PBS. We can estimate the error of the PBS from the single photon counts.
- Not only a VV experiment will result in a single photon dip. For the HV and VH configuration, measurements show it is possible to measure the single photon dip. However, the number of coincidence counts is much less than for VV.
- The lowest dip depth of the VV configuration for $g^{(2)}$ through our “No loop” setup is 0.38, which is limited by the detector response.

5.2 Delay loop setup (one round trip R)

In this section we investigate the loop effect of the delay loop setup, with 1 round trip R in a loop before entering the HBT setup. The scheme of this setup is given in figure 5.4. This setup is almost the physical equivalence of a **Mach-Zehnder interferometer**, where a light beam is split into two by a BS and recombined at another BS. In our setup this is done by one polarizing beam splitter PBS. The first letter and second letter of the polarization configuration are the detected polarizations of detector A and B.

Patel et al. (2008) [29] used this Mach-Zehnder interferometer to demonstrate, by post-selection, the indistinguishability of single photons. In the paper, we see the effect of parallel polarization, see figure 5.5, and orthogonal polarization input in the HBT setup on $g^{(2)}(\tau)$. Proux et al. (2015) [32] repeat this experiment and introduce a coalescence

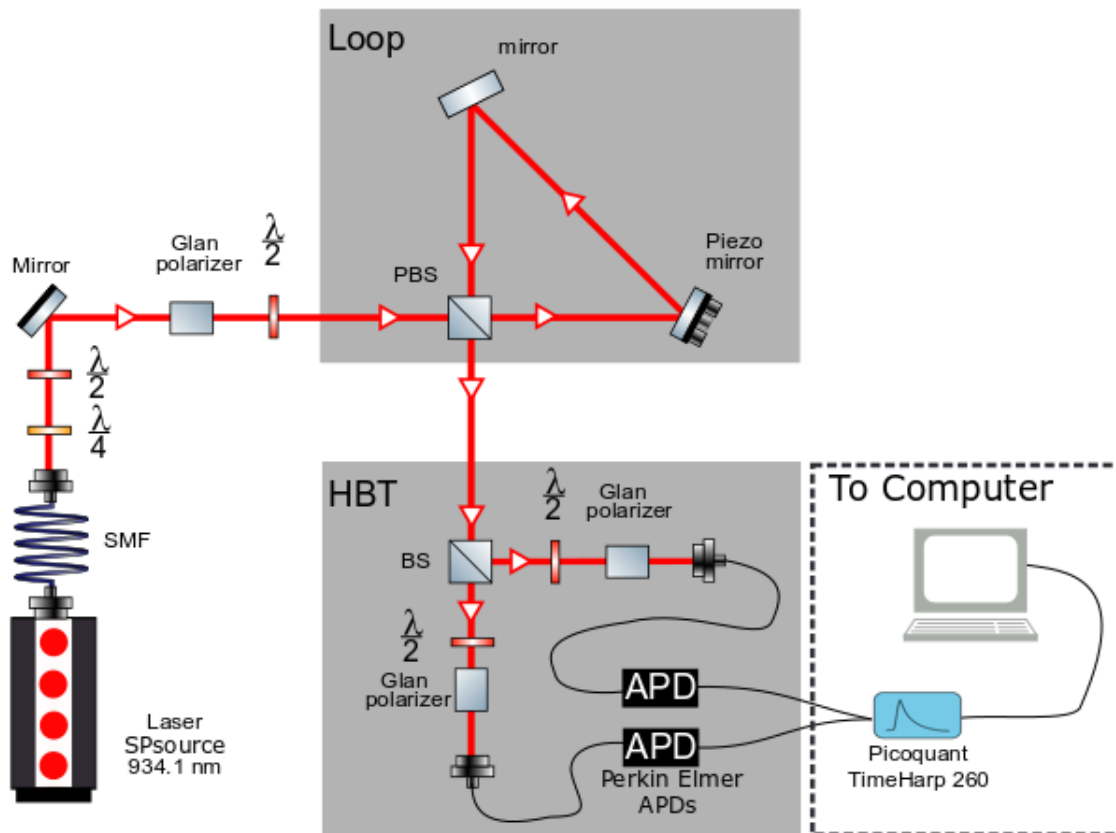


Figure 5.4: Scheme of the HBT setup for the Delay loop setup experiment with the quantum dot single photon source light entering various optical elements. There is no $\frac{\lambda}{2}$ -wave plate in the loop.

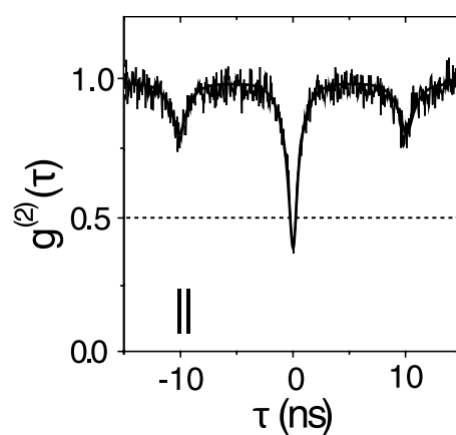


Figure 5.5: HBT and two-photon interference results for the Mach-Zehnder interferometer with parallel polarization between input photons. Three dips are visible, one single photon dip and two 'delay dips'. Figure is taken from the paper from Patel [29], FIG. 3.

time window (CTW) to measure the temporal indistinguishability of single photons by continuous wave excitation of the quantum dot. Both papers show a single photon dip and two 'delay dips' for this setup. In the next section we try to predict the outcome of our experiment and compare with the results from these papers.

5.2.1 Delay loop (one round trip R) prediction

This prediction is based on a stream of photons from quantum dot excitation by a continuous wave laser (CW). Results are described in creation operator notation acting on vacuum state. We assume that the photons are perfectly indistinguishable.

Two photon input

Here \hat{P}_t^\dagger is the quantum state creation operator, with time t and polarization P , acting on $|Vac\rangle$ and time $t = R$ is the duration of one round trip. For the $\frac{\lambda}{2}$ -wave plate we use equations 3.1 and 3.2.

After the $\frac{\lambda}{4}$ -wave plate and $\frac{\lambda}{2}$ -wave plate, incoming light gets horizontally polarized by the polarizer. Assuming interference, thus a tensor product, between photons that go one round trip through the PBS with time $t = R$ and incoming photons in the PBS with $t = R$:

$$\hat{H}_t^\dagger \quad (5.2)$$

$$\xrightarrow{\text{WP}} \frac{1}{\sqrt{2}}(\hat{H}_t^\dagger + \hat{V}_t^\dagger) \quad (5.3)$$

$$\xrightarrow{\text{1 Roundtrip + 2nd photon}} \frac{1}{\sqrt{2}}(\hat{H}_{t+R}^\dagger + \hat{V}_t^\dagger) \otimes \frac{1}{\sqrt{2}}(\hat{H}_{t+R}^\dagger + \hat{V}_{t+R}^\dagger) \quad (5.4)$$

$$\xrightarrow{\text{1 Roundtrip}} \frac{1}{\sqrt{2}}(\hat{H}_{t+R}^\dagger + \hat{V}_t^\dagger) \otimes \frac{1}{\sqrt{2}}(\hat{H}_{t+2R}^\dagger + \hat{V}_{t+R}^\dagger) \quad (5.5)$$

$$= \frac{1}{2} \left(\hat{H}_{t+R}^\dagger \hat{H}_{t+2R}^\dagger + \hat{H}_{t+R}^\dagger \hat{V}_{t+R}^\dagger + \hat{V}_t^\dagger \hat{H}_{t+2R}^\dagger + \hat{V}_t^\dagger \hat{V}_{t+R}^\dagger \right). \quad (5.6)$$

Using this prediction method for one round trips we can create the following table 5.2. The time difference between the incoming photons is equal to the length of the loop, $t = R$. With the prediction we can predict the detection probabilities of the experiment.

Time difference (R)	Photon configuration	Det. Probability
1, -1	HH	$\frac{1}{4}$
-2, 0, 2	HV, VH	$\frac{1}{2}$
1, -1	VV	$\frac{1}{4}$

Table 5.2: Table containing the predicted configurations, for one round trips, with time differences and detection probabilities. For this calculation the input time difference is R .

For HH and VV detection.

Detection probability at $|\tau| = 0$ sec:

$$P_{HH} = P_{VV} = 0. \quad (5.7)$$

Detection probability at $|\tau| = R$ sec:

$$P_{HH} = P_{VV} = \frac{1}{4}. \quad (5.8)$$

For HV and VH detection.

Detection probability at $|\tau| = 0$ sec:

$$P_{HV} = P_{VH} = \frac{1}{4}. \quad (5.9)$$

Detection probability at $|\tau| = R$ sec:

$$P_{HV} = P_{VH} = 0. \quad (5.10)$$

Detection probability at $|\tau| = 2R$ sec:

$$P_{HV} = P_{VH} = \frac{1}{4}. \quad (5.11)$$

Predictions

- For the HH and VV configuration we expect a dip at a time difference of $|\tau| = 0$ for the correlation measurement.
- For the HV and VH configuration we expect a dip at a time difference of $|\tau| = R$ for the correlation measurement.
- The time difference between the dips for the HV and VH configuration will be 2 round trips as we can see in equation 5.6.

5.2.2 Delay loop (one round trip R) experiment

For this experiment we couple light from the quantum dot setup and start the delay loop setup (one round trip R) experiment. Now we can test the prediction with our setup. A scheme for the setup can be seen in figure in figure 5.4. See table 5.3 and 5.4 for all the properties of the VV, HV, VH and HH configuration measurement for the aligned and misaligned case.

In figure 5.6 and tables 5.3 and 5.4 we can see the results of our experiment for the HH and VV configuration. There is dip at $\tau = 0$ for both configurations. For the VV configuration misalignment shows a higher dip depth the HH configuration misalignment shows a lower dip depth.

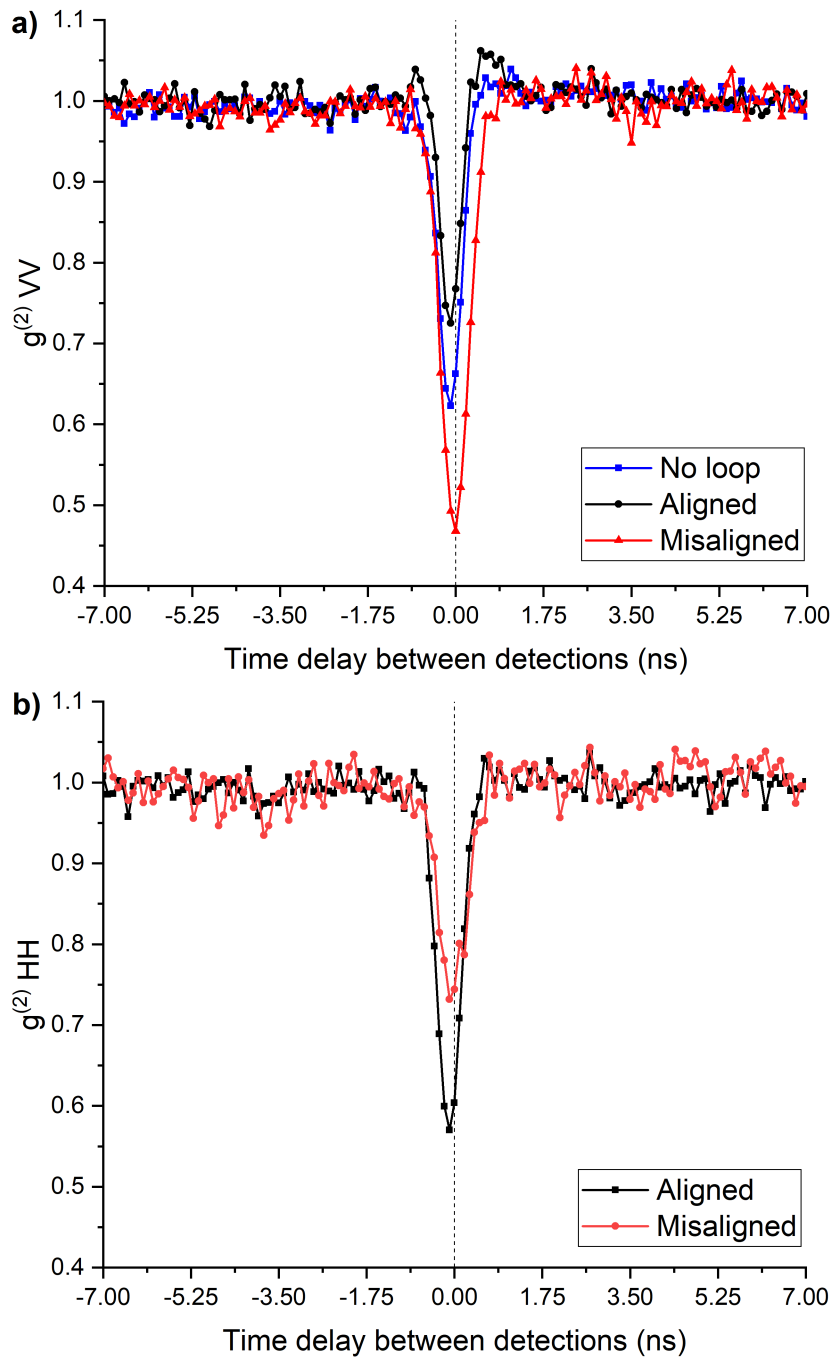


Figure 5.6: $g^{(2)}$ vs the time delay between detections for the VV (a) and HH (b) configuration in the delay loop setup experiment. $g^{(2)}$ with misalignment is also added in red. See table 5.3 and 5.4

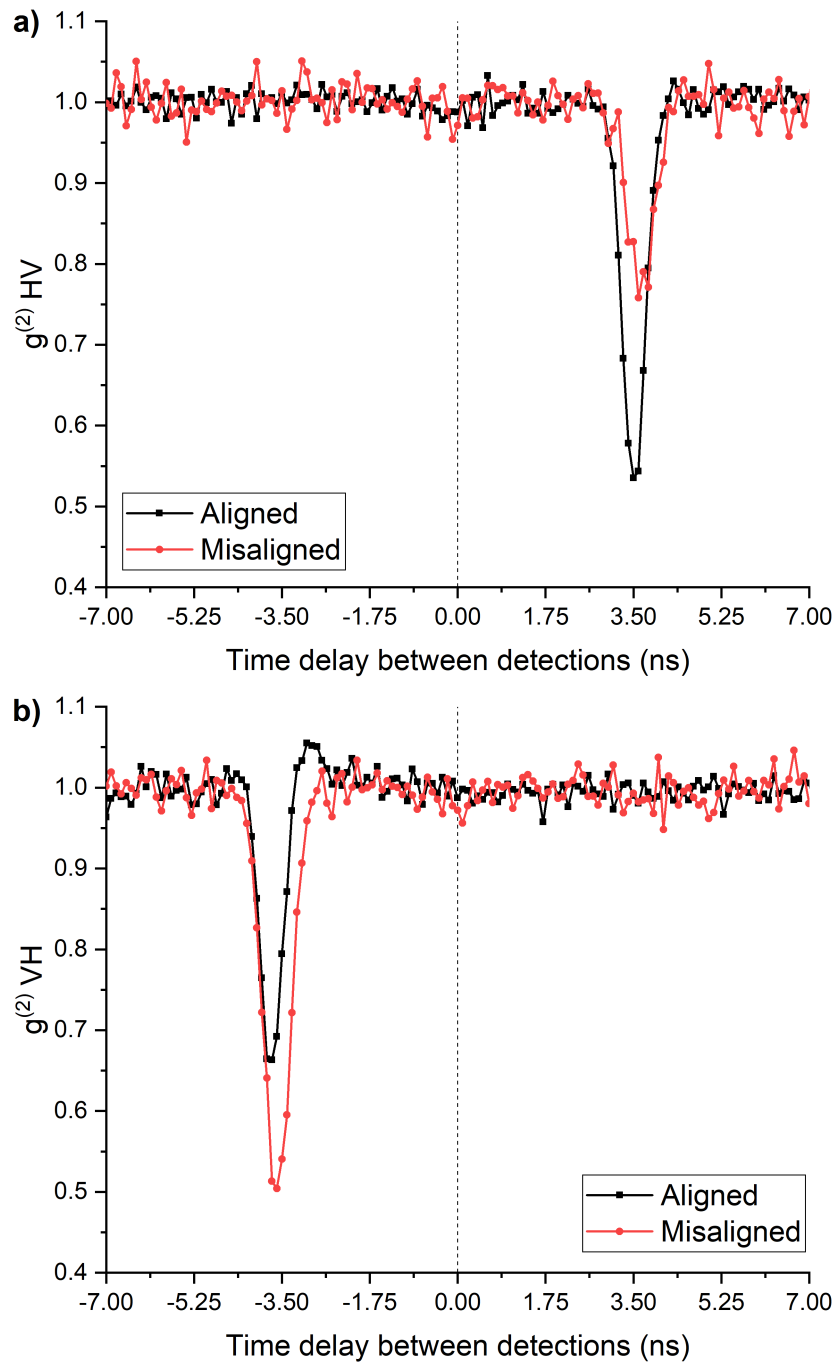


Figure 5.7: $g^{(2)}$ vs the time delay between detections for the HV (a) and VH (b) configuration in the delay loop setup experiment. $g^{(2)}$ with misalignment is also added in red. See table 5.3 and 5.4

Detector A,B	HH	HV	VH	VV
Duration	50 min	50 min	50 min	50 min
#coincidences($\tau \gg 0$)	7526	9855	6737	7742
SP counts (at A)	1.6e5	1.4e5	1.4e5	1.8e5
Normalization	$\frac{\#coincidences}{7526}$	$\frac{\#coincidences}{9855}$	$\frac{\#coincidences}{6737}$	$\frac{\#coincidences}{7742}$
Parameters $\tau_0, A,$	-0.22, 0.29	3.43, 0.29	-3.89, 0.25	-0.45, 0.25
Parameters σ, λ	$\infty, 0.20$	29.08, 0.22	$\infty, 0.19$	$\infty, 0.21$
$g^{(2)}(0)$	0.66	0.97	0.98	0.78
$g^{(2)}(-3.5), g^{(2)}(3.5)$	0.96, 0.97	0.98, 0.64	0.73, 0.97	0.98, 0.99

Table 5.3: Table containing the **Aligned** properties of HH, HV, VH and VV configuration for the delay loop setup experiment. See figure 5.6 and 5.7. Data for the visibilities is not collected.

Detector A,B	HH	HV	VH	VV
Duration	50 min	50 min	50 min	50 min
#coincidences($\tau \gg 0$)	2685	3200	2787	5414
SP counts (at A)	8e4	7e4	1.2e5	1.3e5
Det. A polarization	H	H	V	V
Det. B polarization	H	V	H	V
Normalization	$\frac{\#coincidences}{2685}$	$\frac{\#coincidences}{3200}$	$\frac{\#coincidences}{2787}$	$\frac{\#coincidences}{5414}$
Parameters $\tau_0, A,$	-0.65, 0.15	3.35, 0.14	-3.39, 0.21	-0.31, 0.23
Parameters σ, λ	$\infty, 0.19$	29.44, 0.21	$\infty, 0.17$	30.13, 0.18
$g^{(2)}(0)$	0.76	0.96	0.96	0.56
$g^{(2)}(-3.5), g^{(2)}(3.5)$	0.94, 0.97	0.97, 0.79	0.59, 0.95	0.97, 0.95

Table 5.4: Table containing the **Misaligned** properties of HH, HV, VH and VV configuration for the delay loop setup experiment. See figure 5.6 and 5.7. Data for the visibilities is not collected.

In figure 5.7 and tables 5.3 and 5.4 we can see the results of our experiment for the HV and VH configuration. There is dip at $\tau = 3.5$ for the HV configuration. There is dip at $\tau = -3.5$ for the VH configuration. For the VH configuration misalignment shows a higher dip depth the HV configuration misalignment shows a lower dip depth.

Conclusions

- For the HH and VV configuration we see a dip at a time difference of $|\tau| = 0$ for the correlation measurement, as predicted.
- For the HV and VH configuration we see a dip at a time difference of $|\tau| = R$ for the correlation measurement, as predicted.
- The time difference between the dips for the HV and VH configuration is 2 round trips, as predicted.

- In figure 5.6a the dip depth for the misaligned case is deeper than for the aligned case. Figure 5.6b shows the opposite. Also figure 5.7a and b, should have the same dip depth with misalignment. This is an interesting result, we think it is related to a recent study of Loredó et al. (2018) [22].

Cluster States and indistinguishability

In this chapter a specially designed loop setup is used for the generation of cluster states. We first introduce the cluster states, then we create a prediction and perform experiments for various degrees of photon indistinguishability.

6.1 Cluster states

N-qubit quantum states can be located on a lattice with d dimensions. This lattice is needed to realize **Cluster states**, which are highly entangled qubits, from a Hamiltonian as is shown by Briegel and Raussendorf [6]. Photons, existing in a quantum superposition of polarization states, can be seen as qubits (two-level quantum systems). Qubits can be described in the 'computational basis', given by $\{|0\rangle, |1\rangle\}$. For two qubits the basis of the corresponding 'tensor space' is $|00\rangle, |01\rangle, |10\rangle$ and $|11\rangle$. One can think of photons in a linear cluster state to be produced by a Hamiltonian interaction for a short range [6].

$$H_{int} = \hbar g(t) \sum_{a,a'} f(a-a') \frac{1 + \sigma_z^{(a)}}{2} \frac{1 - \sigma_z^{(a')}}{2}, \quad (6.1)$$

where the Pauli matrix operator $\sigma_z^{(a)}$ (also Pauli-Z operator) acts on the basis vector states as:

$$\sigma_z^{(a)} |0\rangle_a = |0\rangle_a, \quad (6.2)$$

$$\sigma_z^{(a)} |1\rangle_a = -|1\rangle_a. \quad (6.3)$$

Here the indices $a \in \mathbb{Z}^d$ are all occupied lattices sites, $f(a-a')$ is the interaction range, here we only consider next-neighbour interaction, $g(t)$ is a time-dependence term. Translating to quantum information, the interaction Hamiltonian eq. 6.1 can be seen as the Phase shift (R_ϕ) quantum logic gate between the qubits.

1D Example: Linear chain of N qubits

Preparation method introduced by Briegel and Raussendorf (only next-neighbour interaction) [6]. The unitary operator for the interaction hamiltonian takes the form:

$$U(\phi) = \exp\left(\frac{-iH_{int}t}{\hbar}\right) = \exp\left(-ig(t)t \sum_{a,a'} f(a-a') \frac{1+\sigma_z^{(a)}}{2} \frac{1-\sigma_z^{(a')}}{2}\right), \quad (6.4)$$

since we got next-neighbour interaction and $g(t)$ is constant:

$$f(a-a') = \delta_{a+1,a'}, \quad (6.5)$$

$$\phi = \int g(t)dt = gt. \quad (6.6)$$

hence

$$U(\phi) = \exp\left(-i\phi \sum_a \frac{1+\sigma_z^{(a)}}{2} \frac{1-\sigma_z^{(a+1)}}{2}\right), \quad (6.7)$$

where N is the number of qubits in the system. The chain becomes **disentangled** when ϕ takes values: $0, 2\pi, 4\pi, \dots$ and **entangled** for: $\pi, 3\pi, 5\pi, \dots$. Initially all qubit states in the linear chain are given by:

$$|\psi\rangle_a = \frac{|0\rangle_a + |1\rangle_a}{\sqrt{2}}. \quad (6.8)$$

Applying the evolution operator eq. 6.4 on the qubit states using $\phi = \pi$ for an entangled state:

$$\begin{aligned} |\phi_N\rangle &= U(\phi = \pi) |\psi_N\rangle \\ &= \frac{1}{2^{N/2}} \bigotimes_{a=1}^N \left(|0\rangle_a \sigma_z^{(a+1)} + |1\rangle_a \right). \end{aligned} \quad (6.9)$$

This is the formula for linear cluster states, which is the same as equation (2) from [6]. Here we use $\sigma_z^{(N+1)} \equiv 1$, since there is no possibility to entangle with an empty qubit state.

Using the formula for the generation of cluster states, equation 6.9, we can calculate for N qubits the resulting linear cluster state:

- For N = 2 qubits we obtain:

$$|\phi_2\rangle = \frac{1}{2}(|0\rangle_1 \sigma_z^{(2)} + |1\rangle_1)(|0\rangle_2 + |1\rangle_2) = \frac{1}{2}(|0\rangle_1 (|0\rangle_2 - |1\rangle_2) + |1\rangle_1 (|0\rangle_2 + |1\rangle_2)). \quad (6.10)$$

Writing it in the standard form with local unitary transformation:

$$|\phi_2\rangle = \frac{1}{\sqrt{2}}(|0\rangle_1 |0\rangle_2 + |1\rangle_1 |1\rangle_2). \quad (6.11)$$

This is one of the 4 **Bell states**, which is a maximally entangled state. In general the four Bell states are written as

$$|\phi_2\rangle = |\Phi^+\rangle = \frac{1}{\sqrt{2}}(|0\rangle_1 |0\rangle_2 + |1\rangle_1 |1\rangle_2), \quad (6.12)$$

$$|\Phi^-\rangle = \frac{1}{\sqrt{2}}(|0\rangle_1 |0\rangle_2 - |1\rangle_1 |1\rangle_2), \quad (6.13)$$

$$|\Psi^+\rangle = \frac{1}{\sqrt{2}}(|0\rangle_1 |1\rangle_2 + |1\rangle_1 |0\rangle_2), \quad (6.14)$$

$$|\Psi^-\rangle = \frac{1}{\sqrt{2}}(|0\rangle_1 |1\rangle_2 - |1\rangle_1 |0\rangle_2). \quad (6.15)$$

- For N = 3 qubits we obtain:

$$|\phi_3\rangle = \frac{1}{\sqrt{2}}(|0\rangle_1 |0\rangle_2 |0\rangle_3 + |1\rangle_1 |1\rangle_2 |1\rangle_3), \quad (6.16)$$

- For N = 4 qubits we obtain:

$$|\phi_4\rangle = \frac{1}{2}(|0\rangle_1 |0\rangle_2 |0\rangle_3 |0\rangle_4 + |0\rangle_1 |0\rangle_2 |1\rangle_3 |1\rangle_4 + |1\rangle_1 |1\rangle_2 |0\rangle_3 |0\rangle_4 - |1\rangle_1 |1\rangle_2 |1\rangle_3 |1\rangle_4). \quad (6.17)$$

6.2 Cluster state setup prediction

6.2.1 Method

Here we create a prediction for the outcome of the cluster state setup, see figure 6.1, for a stream of photons from quantum dot excitation by a continuous wave laser (CW). Results are described in creation operator notation acting on vacuum state. We assume that the photons are perfectly indistinguishable.

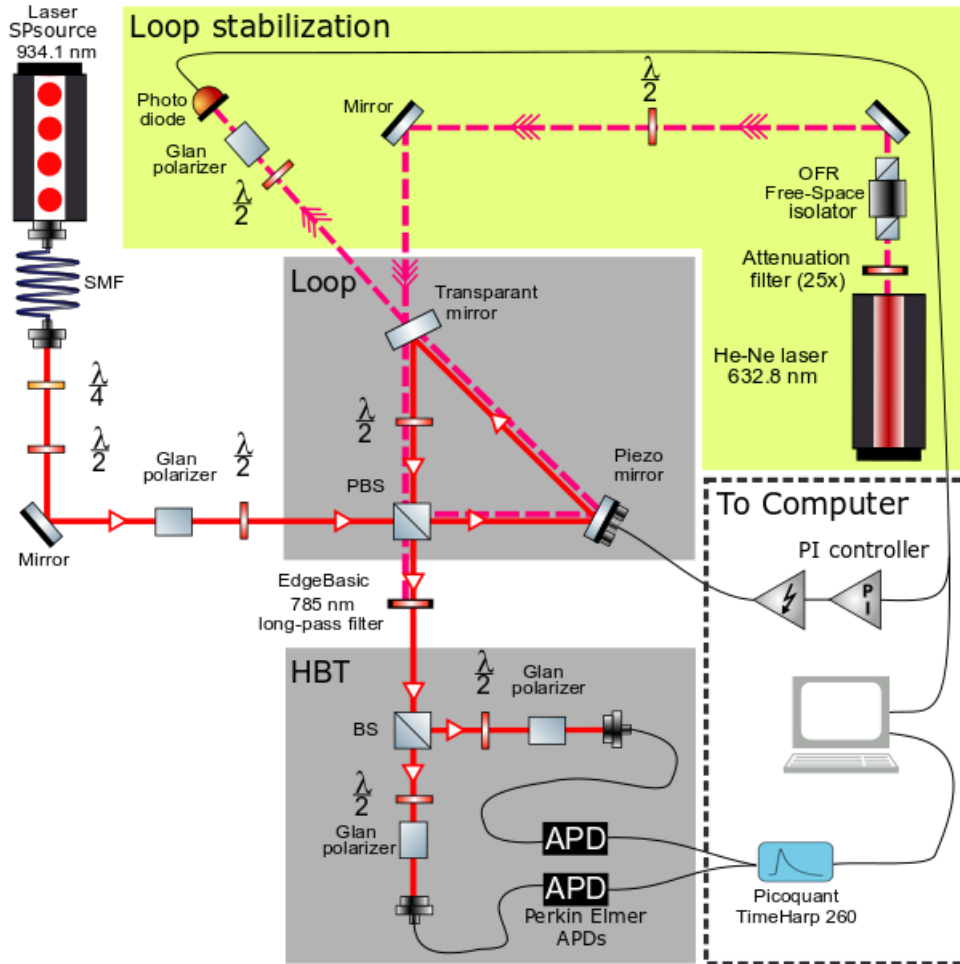


Figure 6.1: Optical setup used in this thesis for the generation of cluster states based on a single photon (SP) source. Arrows in the figure illustrate the direction of the photons and light beams. The SP light passes through a single mode fiber (SMF), through wave plates, polarizers, (polarizing) beam splitters (BS), a Loop and the Perkin Elmer Avalanche Photon Detectors (APD) in the Hanbury Brown & Twiss (HBT) setup. The loop stabilization is done with an attenuated He-Ne laser, that is sent through an optical isolator, before it enters the loop. Data is processed by a computer, which also controls the piezo mirror in the loop with a proportional-integral controller.

6.2.2 Single photon input (red operator in loop)

Here \hat{P}_t^\dagger is the quantum state creation operator, with time t and polarization P , acting on $|Vac\rangle$ and time $t = R$ is the duration of one round trip. Using equations 3.1 and 3.2:

No round trip ($Q_0(t)$):

$$\frac{1}{\sqrt{2}}(\hat{H}_t^\dagger + \hat{V}_t^\dagger). \quad (6.18)$$

1 round trip ($Q_1(t)$):

$$\xrightarrow{\text{WP}} \frac{1}{\sqrt{2}} \left(\frac{1}{\sqrt{2}} (\hat{V}_{t+R}^\dagger + \hat{H}_{t+R}^\dagger) + \hat{V}_t^\dagger \right). \quad (6.19)$$

2 round trips ($Q_2(t)$):

$$\xrightarrow{\text{WP}} \frac{1}{\sqrt{2}} \left(\frac{1}{\sqrt{2}} \left(\frac{1}{\sqrt{2}} (-\hat{V}_{t+2R}^\dagger + \hat{H}_{t+2R}^\dagger) + \hat{H}_{t+R}^\dagger \right) + \hat{V}_t^\dagger \right). \quad (6.20)$$

3 round trips ($Q_3(t)$):

$$\xrightarrow{\text{WP}} \frac{1}{\sqrt{2}} \left(\frac{1}{\sqrt{2}} \left(\frac{1}{\sqrt{2}} \left(\frac{1}{\sqrt{2}} (\hat{V}_{t+3R}^\dagger - \hat{H}_{t+3R}^\dagger) + \hat{H}_{t+2R}^\dagger \right) + \hat{H}_{t+R}^\dagger \right) + \hat{V}_t^\dagger \right). \quad (6.21)$$

4 round trips ($Q_4(t)$):

$$\xrightarrow{\text{WP}} \frac{1}{\sqrt{2}} \left(\frac{1}{\sqrt{2}} \left(\frac{1}{\sqrt{2}} \left(\frac{1}{\sqrt{2}} \left(\frac{1}{\sqrt{2}} (-\hat{V}_{t+4R}^\dagger + \hat{H}_{t+4R}^\dagger) - \hat{H}_{t+3R}^\dagger \right) + \hat{H}_{t+2R}^\dagger \right) + \hat{H}_{t+R}^\dagger \right) + \hat{V}_t^\dagger \right). \quad (6.22)$$

Conclusions

- The same number of single photons reaching the detector is vertically or horizontally polarized.
- Only horizontally polarized light leaves the loop.
- Each round trip R the probability that photons remain in the loop is:

$$P(R) = \left(\frac{1}{2} \right)^{R+1}. \quad (6.23)$$

For two photon interference the two photons must be identical in their spatial, temporal and polarization degrees of freedom. The second photon enters the loop at $t = R, 2R, \dots$

6.2.3 Two photon input with 2 round trips (red operator in loop)

In this example we consider two photon interference with a time difference of 1 round trip. After 1 round trip of the first photon the total quantum state creation operator, acting on $|Vac\rangle$, is:

$$\Psi^+ = Q_1(t) \otimes Q_0(t+R). \quad (6.24)$$

Using Q_0 from equation 6.18 and Q_1 from equation 6.19 and time $t = 0$:

$$Q_1(0) \otimes Q_0(R) = \frac{1}{\sqrt{2}} \left(\frac{1}{\sqrt{2}} \left(\hat{V}_{t+R}^+ + \hat{H}_{t+R}^+ \right) + \hat{V}_t^+ \right) \otimes \frac{1}{\sqrt{2}} \left(\hat{H}_t^+ + \hat{V}_t^+ \right). \quad (6.25)$$

The 2nd round trip of both photons gives

$$Q_2(R) \otimes Q_1(2R) = \frac{1}{\sqrt{2}} \left(\frac{1}{\sqrt{2}} \left(\frac{1}{\sqrt{2}} \left(-\hat{V}_{3R}^+ + \hat{H}_{3R}^+ \right) + \hat{H}_{2R}^+ \right) + \hat{V}_R^+ \right) \otimes \frac{1}{\sqrt{2}} \left(\frac{1}{\sqrt{2}} \left(\hat{V}_{3R}^+ + \hat{H}_{3R}^+ \right) + \hat{V}_{2R}^+ \right) \quad (6.26)$$

After calculation of this tensor product, due to the fact that the commutation relation for bosons is zero, see equation 2.31, the following part stands out:

$$= \left(\hat{H}_{3R}^+ - \hat{V}_{3R}^+ \right) \otimes \left(\hat{H}_{3R}^+ + \hat{V}_{3R}^+ \right) \quad (6.27)$$

$$= \hat{H}_{3R}^+ \hat{H}_{3R}^+ + \hat{H}_{3R}^+ \hat{V}_{3R}^+ - \hat{V}_{3R}^+ \hat{H}_{3R}^+ - \hat{V}_{3R}^+ \hat{V}_{3R}^+ \quad (6.28)$$

$$= \hat{H}_{3R}^+ \hat{H}_{3R}^+ - \hat{V}_{3R}^+ \hat{V}_{3R}^+. \quad (6.29)$$

Using the probabilities, this results in the following quantum entangled Bell state: ^{NB}

$$\frac{1}{4\sqrt{2}} \left(\hat{H}_{3R}^+ \hat{H}_{3R}^+ - \hat{V}_{3R}^+ \hat{V}_{3R}^+ \right) |Vac\rangle \quad (6.30)$$

$$= \frac{1}{\sqrt{2}} (|HH\rangle - |VV\rangle) = |\Phi^-\rangle. \quad (6.31)$$

Which is the cluster state we would like to detect in our setup.

Conclusions

- For a two photon input with quantum interference, we detect one of the maximally entangled Bell states $|\Phi^-\rangle$. Y.Pilnyak et al. (2017) [30] suggest here to ignore the rest of the results and use postselection.
- We can generate the total quantum state creation operator for each configuration of photons with different time differences.

NB: Normalization of the resultant quantum state is preserved due to the fact that creation operators squared (spatial, temporal and polarization identical) acting on vacuum will give an extra factor $\sqrt{2}$, see equation 2.17.

6.2.4 Prediction after 3 round trips

Using this prediction method for 3 round trips we can create the following table 6.1. The time difference between the incoming photons is equal to the length of the loop, $t = R$. With the prediction we can predict the detection probabilities of the experiment. Here we used $Q_1(t) \otimes Q_0(t + R)$ for the prediction, developed for 3 round trips.

For VV detection.

Here the extra $\frac{1}{2}$ comes from the beam splitter in the HBT setup:

Detection probability at $|\tau| = 0$ sec:

$$P_{VV} = 0. \quad (6.32)$$

Detection probability at $|\tau| = R$ sec:

$$P_{VV} = \frac{1}{2} \left(\frac{\frac{1}{4}}{\frac{1}{4} + \frac{1}{16} + \frac{1}{16}} \right) = \frac{1}{3}. \quad (6.33)$$

For HH detection.

Here the extra $\frac{1}{2}$ comes from the beam splitter in the HBT setup:

Detection probability at $|\tau| = 0$ sec:

$$P_{HH} = \frac{1}{2} \left(\frac{\frac{1}{16} + \frac{1}{64}}{\frac{1}{8} + \frac{1}{16} + \frac{1}{64} + \frac{1}{64} + \frac{1}{64} + \frac{1}{64}} \right) = \frac{5}{32}. \quad (6.34)$$

Detection probability at $|\tau| = R$ sec:

$$P_{HH} = \frac{1}{2} \left(\frac{\frac{1}{16}}{\frac{1}{4} + \frac{1}{16} + \frac{1}{16}} \right) = \frac{1}{12}. \quad (6.35)$$

Time difference (R)	Photon 1	Photon 2	Det. Probability	HH det.	VV det.
0	H	V	$\frac{1}{8}$	-	-
0	H	H	$\frac{1}{16}$	Yes	-
0	H	H	$\frac{1}{64}$	Yes	-
0	H	V	$\frac{1}{64}$	-	-
0	V	H	$\frac{1}{64}$	-	-
0	V	V	$\frac{1}{64}$	-	-
1, -1	V	V	$\frac{1}{4}$	-	Yes
1, -1	H	H	$\frac{1}{16}$	Yes	-
1, -1	H	V	$\frac{1}{16}$	-	-
2, -2	V	H	$\frac{1}{8}$	-	-
2, -2	H	V	$\frac{1}{32}$	-	-
2, -2	V	V	$\frac{1}{32}$	-	-
2, -2	H	H	$\frac{1}{32}$	Yes	-
2, -2	H	V	$\frac{1}{32}$	-	-
3, -3	V	H	$\frac{1}{16}$	-	-
3, -3	V	V	$\frac{1}{16}$	-	-
			Total = 1		

Table 6.1: Table containing the predicted configurations, for 3 round trips, with time differences and detection probabilities. For this calculation the input time difference is R and the input is a single photon Fock state. Yes in the column for HH and VV configuration means that the state can be detected.

Predictions

- For the VV configuration we expect a dip at a time difference of $|\tau| = 0$ for the correlation measurement.
- For the HH configuration we expect dips at a time difference of $|\tau| = R$ that are $\frac{5}{12} \approx 2$ times bigger than a dip at $|\tau| = 0$
- The dip depth at $|\tau| = 0$ is for the VV configuration bigger than HH.
- The dip depth at $|\tau| = R$ is for the HH configuration bigger than VV.

6.3 Cluster state setup experiment 1

For this experiment we couple light from the quantum dot setup and start the cluster state setup experiment 1. Now we can test the prediction with our setup. A scheme for the setup can be seen in figure 6.1. The length of a round trip here is $R = 3.5$ ns. See table 6.2 for all the properties of the VV and HH configuration measurement. The first letter and second letter of the polarization configuration are the detected polarizations

Detector A,B	VV (94%)	HH (94%)	VV (46%)	HH (46%)
Duration	50 min	50 min	50 min	50 min
#coincidences($\tau \gg 0$)	13949	9700	2801	2323
SP counts (at A)	2e5	1.5e5	1e5	5e4
Det. A visibility	96%	96%	42%	42%
Det. B visibility	92%	92%	49%	49%
Normalization	$\frac{\#coincidences}{13949}$	$\frac{\#coincidences}{9700}$	$\frac{\#coincidences}{2801}$	$\frac{\#coincidences}{2323}$
Parameters $\tau_0, A,$	-0.24, 0.18	-0.64, 0.11	-0.35, 0.22	-0.04, 0.17
Parameters σ, λ	$\infty, 0.17$	17.09, 0.11	4139.52, 0.19	16.14, 0.11
$g^{(2)}(0)$	0.69	0.95	0.82	0.87
$g^{(2)}(-3.5), g^{(2)}(3.5)$	0.96, 0.98	0.89, 0.89	0.96, 0.97	0.94, 0.90

Table 6.2: Table containing the properties of HH and VV configuration for the cluster state setup experiment 1 for a visibility of 94% and 46%. See figure 6.2a and b.

Detector A,B	VV (67%)	VV (37%)	VV (10%)	HH (67%)	HH (37%)	HH (10%)
Duration	50 min	50 min	50 min	50 min	50 min	50 min
#c.c.($\tau \gg 0$)	20243	24190	2357	13196	8744	879
SP counts (at A)	3.4e5	3e5	6e4	2.2e5	1.6e5	5e4
Det. A vis.	63%	33%	9%	63%	33%	9%
Det. B vis.	71%	40%	10%	71%	40%	10%
Norm.	$\frac{\#coincidences}{20243}$	$\frac{\#coincidences}{24190}$	$\frac{\#coincidences}{2357}$	$\frac{\#coincidences}{13196}$	$\frac{\#coincidences}{8744}$	$\frac{\#coincidences}{879}$
Parameters $\tau_0, A,$	-0.38, 0.27	-0.20, 0.35	-0.11, 0.36	-0.68, 0.16	-0.57, 0.19	0.48, 0.21
Parameters σ, λ	$\infty, -0.38$	$\infty, 0.18$	$\infty, 0.20$	12.17, 0.08	14.65, 0.09	10.05, 0.08
$g^{(2)}(0)$	0.75	0.57	0.57	0.89	0.88	0.83
$g^{(2)}(-3.5)$	0.97	0.98	0.97	0.88	0.91	0.87
$g^{(2)}(3.5)$	0.99	1.00	0.99	0.89	0.92	0.87

Table 6.3: Table containing the properties of HH and VV configuration for the cluster state setup experiment 2 for a visibility of 67%, 37% and 10%. See figure 6.3a and b.

of detector A and B. In figure 6.2a we can see the results of our experiment.

Conclusions

- For the VV configuration we see a dip at a time difference of $|\tau| = 0$, with a dip depth of 0.31, for the correlation measurement, as predicted.
- For the HH configuration we see dips at a time difference of $|\tau| = R$ that are $\frac{0.11}{0.05} \approx 2$ times bigger than a dip at $|\tau| = 0$, as predicted.
- The dip depth at $|\tau| = 0$ is for the VV configuration bigger than HH, $0.31 < 0.05$, as predicted.

- The dip depth at $|\tau| = R$ is for the HH configuration bigger than VV, $0.11 < 0.04$, as predicted.

6.4 Cluster state setup experiment 2

For this experiment we couple light from the quantum dot setup and start the cluster state setup experiment 2. However now we misalign this setup in steps. A scheme for the setup can be seen in figure 6.1. The length of a round trip here is $R = 3.5$ ns. We call the dip depth at τ : dip depth = $(1 - g^{(2)}(\tau))$. As we can see in the figure 6.2a and 6.2b the depth of the dips at zero for the HH and VV configuration, change as a function of the visibility. The first letter and second letter of the polarization configuration are the detected polarizations of detector A and B. For dips at $|\tau| = 3.5$ we see small differences. We now would like to test this behavior at $|\tau| = 0$ for 5 different visibilities by misaligning the PBS in the Loop setup. The visibilities we used in this experiment are: $V \approx 94\%$, 67% , 46% , 37% and 10% . The measurement results for a visibility of $V \approx 50\%$ are plotted in figure 6.2b. See the tables 6.2 and 6.3 for all the properties of the VV and HH configuration measurements. All measurements were done on the 19th of June (2019).

To compare the visibilities and number of coincidences as a function of the visibility we plot this information for the HH configuration in figure 6.3. When starting the $V \approx 50\%$ measurements the loop could not be locked properly, the lock uses the interference in the loop and for reduced visibility it is not possible to lock the loop. So for the visibilities $V \approx 50\%$, 35% and 10% the loop is not locked.

Conclusions

- For the HH configuration the $g^{(2)}(0)$ can be approximated as a function of the visibility,

$$g_{\text{HH}}^{(2)}(0) \approx 0.12 (\text{Visibility}) + 0.82, \quad (6.36)$$

with a Standard error (SE) of 0.02 and an error of $\approx 4\%$ (0.04) for the visibility. The coefficient of determination, R-Square, is ≈ 0.93 .

- As already argued for the loop with one round trip we expect that for the VV configuration the dip depth at τ is affected by misalignment. We speculate that the reason for this difference is the excitation of a different quantum dot.

Discussion

Have we measured two-photon cluster states? We found a relationship between the dip depth at $|\tau| = 0$ as a function of the visibility, so we expect that the alignment of the setup creates this maximum entangled bell pair of equation 6.13, which is an indication of the creation of cluster states. However, further investigation is needed to confirm this result.

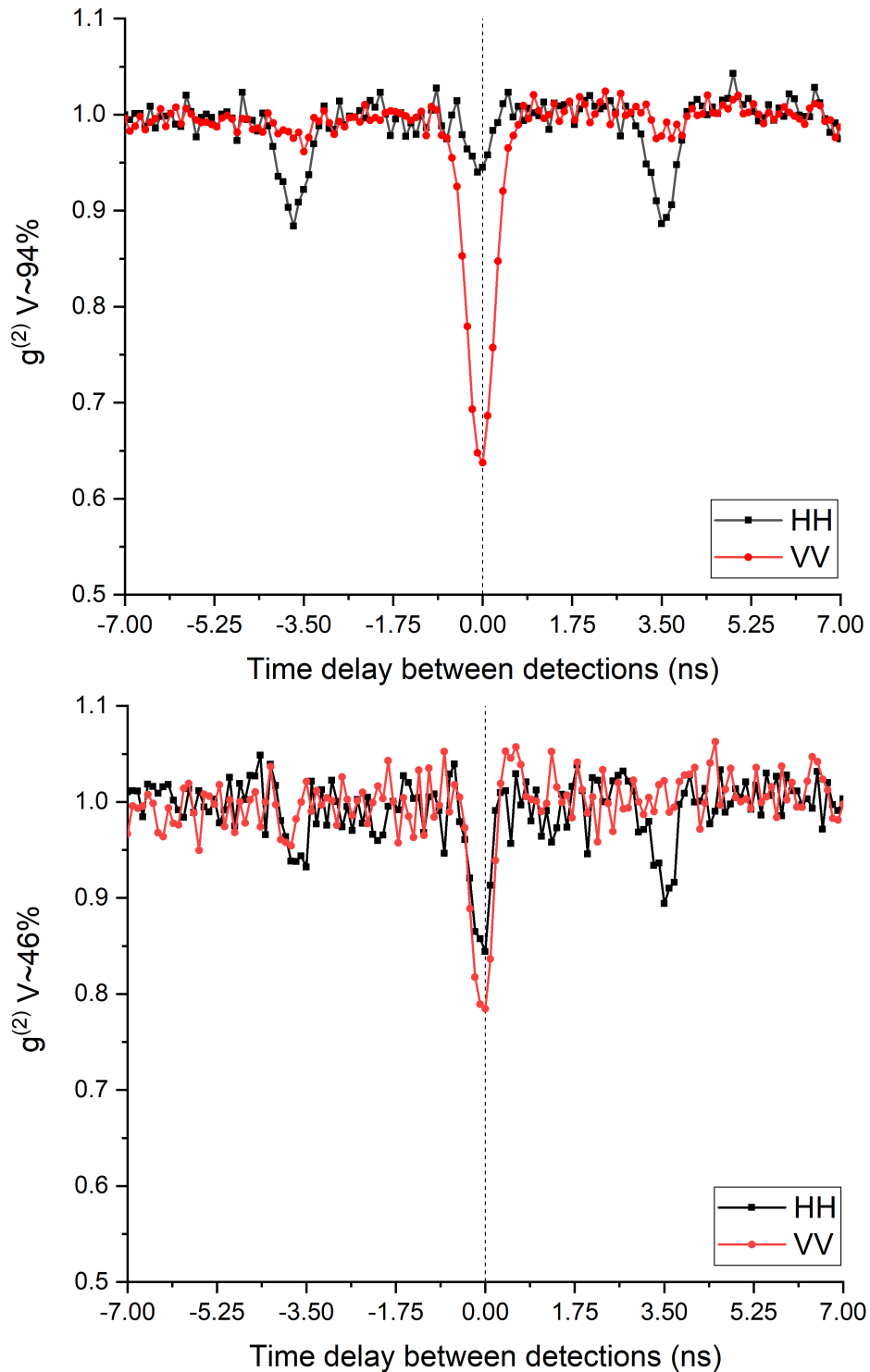


Figure 6.2: HH and VV configuration in the cluster state setup experiment 1. a) The visibility of the measurement is approximately 94%. b) The visibility of the measurement, due to misalignment of the PBS, is approximately 46%. See table 6.2.

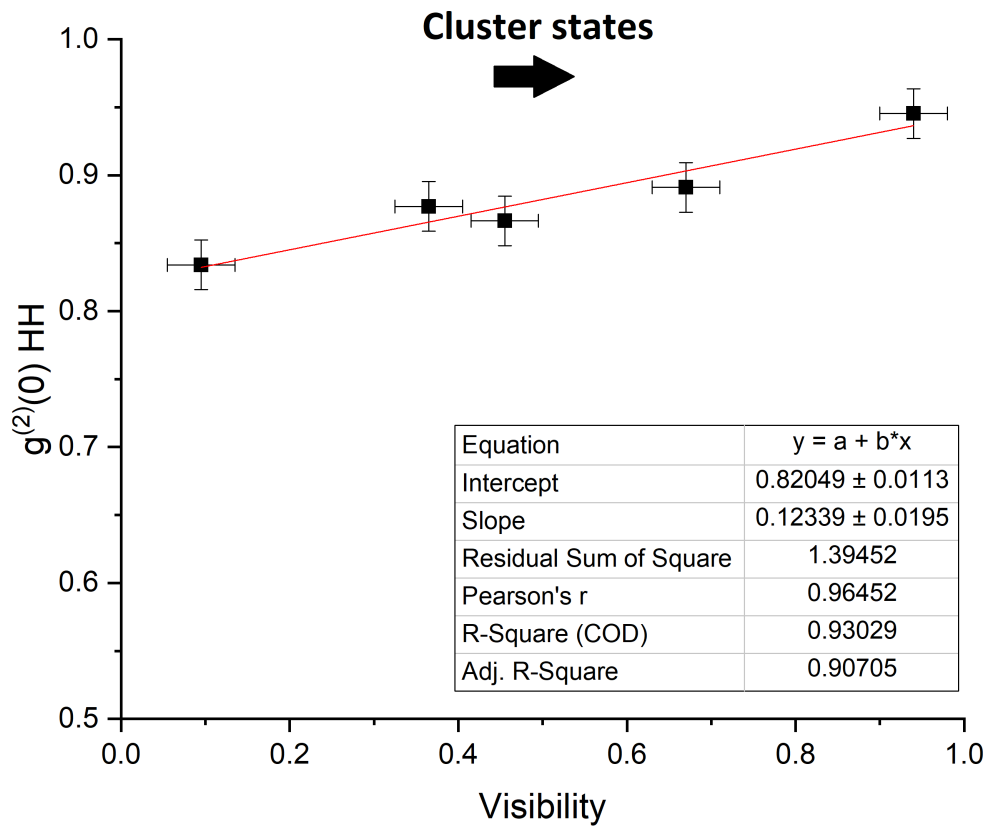


Figure 6.3: $g^{(2)}(0)$ for the HH configuration for 5 different visibilities, with errors indicated. The red line is a fit through these data points. See table 6.3.

Conclusion

7.1 Research questions

How does a change in the properties of the quantum optical single photon source affect the indistinguishability?

We see that our normalization results for the Hanbury Brown and Twiss setup with only the quantum dot source results in a single photon purity of $\approx 60\%$, which is because of the detector response and jitter.

Which consequences does a spatial or temporal misalignment have on the quantum interference in the cluster state loop setup?

Spatial misalignment can decrease the number of single photons entering the loop (or going one round trip), only for horizontally polarized photons in our setup. For two photon quantum interference the two photons must be identical in their spatial, temporal and polarization degrees of freedom. Our results show that quantum interference happens when the time between the single photons matches the time of the delay loop for the cluster state setup. For the HH configuration the dip depth can be approximated as a function of the visibility.

What impact have partial distinguishable single photons on the quantum information processing with quantum entangled qubits in cluster states?

For a two photon input with quantum interference, we should be able to detect, by post-selection, one of the maximally entangled Bell states $|\Phi^-\rangle$. However, at this moment, we can only predict with analytical software. We could not find a relation between the number of coincidences and the dips for partial distinguishable photons.

Acknowledgements

From start to finish of my project I was feeling welcome in the Quantum Optics research group of my supervisor, the Quphotonics group. Therefore I would like to offer my profound thanks to **Dr. Wolfgang Löffler**. This work was accomplished due to his provision of continuous support, motivation and supervision. I am also **Dr. Vedran Dunjko** very thankful for considering my request to be a second supervisor.

In my day-to-day work my most humble thanks goes in particular to PhD student **Petr Steindl**, for the help, normalization of results and execution of experiments, to BSc student **Edward Hissink** for the fruitful discussions and working together on the experimental setup and also **Dr. Henk Snijders** for his encouragement, knowledge and expertise in the field of Cavity Quantum ElectroDynamics (CQED), Quantum Dots and Single Photons. He helped me to solve difficult analytical and technical problems.

Finally my special thanks goes to my family and all colleagues of the quantum optics group. Their extra support helped me to present this work.

Bibliography

- [1] M.P. Bakker. *Cavity quantum electrodynamics with quantum dots and solid-state cavities*. Doctoral thesis, Leiden University, 2015.
- [2] L.E. Ballentine. *Quantum Mechanics: A Modern Development*. World Scientific, 1998.
- [3] T. Banks. *Quantum Mechanics: An Introduction*. CRC Press, 2018.
- [4] E. Barsky. *Gibbs' Entropic Paradox and Problems of Separation Processes*. Elsevier Science, 2017.
- [5] A.M. Branczyk. *Hong-Ou-Mandel Interference*, 2017.
- [6] Hans J. Briegel and Robert Raussendorf. Persistent entanglement in arrays of interacting particles. *Phys. Rev. Lett.*, 86:910–913, Jan 2001.
- [7] Katiúscia N. Cassemiro, Kaisa Laiho, and Christine Silberhorn. Accessing the purity of a single photon by the width of the Hong-Ou-Mandel interference. *New Journal of Physics*, 12, 2010.
- [8] P.A.M. Dirac. *The Principles of Quantum Mechanics*. Clarendon Press, Oxford, 3rd edition, 1954.
- [9] Albert Einstein. Über einen die Erzeugung und Verwandlung des Lichtes betreffenden heuristischen Gesichtspunkt. *Annalen der Physik*, 1905.
- [10] M. Fox. *Quantum Optics - An Introduction*. Oxford University Press, Oxford, 2006.
- [11] A.P. French and E.F. Taylor. *An introduction to quantum physics*. M.I.T. introductory physics series. Nelson, 1979.
- [12] C. Gerry, P. Knight, and P.L. Knight. *Introductory Quantum Optics*. Cambridge University Press, 2005.
- [13] Roy J. Glauber. The quantum theory of optical coherence. *Phys. Rev.*, 130:2529–2539, Jun 1963.

-
- [14] R. Hanbury Brown and R. Q. Twiss. A Test of a New Type of Stellar Interferometer on Sirius. 178:1046–1048, November 1956.
- [15] C. K. Hong, Z. Y. Ou, and L. Mandel. Measurement of subpicosecond time intervals between two photons by interference. *Phys. Rev. Lett.*, 59:2044–2046, Nov 1987.
- [16] J.M. Jauch. *Foundations of Quantum Mechanics*. Addison-Wesley Publishing Company, Geneva, 1968.
- [17] MIT Kerson Huang. *Statistical Mechanics*, 1987.
- [18] K. Konishi and G. Paffuti. *Quantum mechanics: a new introduction*. Oxford University Press, 2009.
- [19] L.D. Landau and E.M. Lifshitz. *Course of Theoretical Physics*. Elsevier Science, 2013.
- [20] N. H. Lindner, D. Cogan, O. Kenneth, E. R. Schmidgall, D. Gershoni, I. Schwartz, Y. Don, and L. Gantz. Deterministic generation of a cluster state of entangled photons. *Science*, 354(6311):434–437, 2016.
- [21] Netanel H. Lindner and Terry Rudolph. Proposal for pulsed on-demand sources of photonic cluster state strings. *Phys. Rev. Lett.*, 103:113602, Sep 2009.
- [22] J. C. Loredó, C. Antón, B. Reznichenko, P. Hilaire, A. Harouri, C. Millet, H. Olivier, N. Somaschi, L. De Santis, A. Lemaître, I. Sagnes, L. Lanco, A. Auffèves, O. Krebs, and P. Senellart. Generation of non-classical light in a photon-number superposition. pages 1–13, 2018.
- [23] L. Mandel. Coherence and indistinguishability. *Optics Letters*, 16(23):1882, 1991.
- [24] L. Mandel, E. Wolf, and Cambridge University Press. *Optical Coherence and Quantum Optics*. Cambridge University Press, 1995.
- [25] F. Mandl. *Quantum Mechanics*. Manchester Physics Series. Wiley, 2013.
- [26] A. M. L. Messiah and O. W. Greenberg. Symmetrization postulate and its experimental foundation. *Phys. Rev.*, 136:B248–B267, Oct 1964.
- [27] R. Mirman. Experimental meaning of the concept of identical particles. *Nuovo Cim., B, v. 18B, no. 1, pp. 110-122*, 11 1973.
- [28] M. Orszag. *Quantum Optics*. Advanced texts in physics. Springer, 2000.
- [29] R. B. Patel, A. J. Bennett, K. Cooper, P. Atkinson, C. A. Nicoll, D. A. Ritchie, and A. J. Shields. Postselective two-photon interference from a continuous nonclassical stream of photons emitted by a quantum dot. *Phys. Rev. Lett.*, 100:207405, May 2008.

-
- [30] Y. Pilnyak, N. Aharon, D. Istrati, E. Megidish, A. Retzker, and H. S. Eisenberg. Simple source for large linear cluster photonic states. *Physical Review A*, 95(2):1–12, 2017.
- [31] Max Planck. über das gesetz der energieverteilung im normalspectrum. *Annalen Der Physik*, 309, 01 1901.
- [32] Raphaël Proux, Maria Maragkou, Emmanuel Baudin, Christophe Voisin, Philippe Roussignol, and Carole Diederichs. Measuring the photon coalescence time window in the continuous-wave regime for resonantly driven semiconductor quantum dots. *Phys. Rev. Lett.*, 114:067401, Feb 2015.
- [33] Charles Santori, Glenn S Solomon, David Fattal, Jelena Vuc, and Yoshihisa Yamamoto. Indistinguishable photons from a single-photon device. *Nature*, 395(6697):16, 1998.
- [34] H. J. Snijders. *Quantum dot microcavity control of photon statistics*. Doctoral thesis, Leiden University, 2018.
- [35] R. M. Stevenson, C. L. Salter, J. Nilsson, A. J. Bennett, M. B. Ward, I. Farrer, D. A. Ritchie, and A. J. Shields. Indistinguishable entangled photons generated by a light-emitting diode. *Phys. Rev. Lett.*, 108:040503, Jan 2012.
- [36] E. C. G. Sudarshan. Equivalence of semiclassical and quantum mechanical descriptions of statistical light beams. *Phys. Rev. Lett.*, 10:277–279, Apr 1963.
- [37] F. W. Sun and C. W. Wong. Indistinguishability of independent single photons. *Physical Review A - Atomic, Molecular, and Optical Physics*, 79(1):1–6, 2009.
- [38] R. Swendsen. Statistical mechanics of colloids and boltzmann’s definition of the entropy. *American Journal of Physics - AMER J PHYS*, 74, 03 2006.
- [39] D. Valente, F. Brito, R. Ferreira, and T. Werlang. Work on a quantum dipole by a single-photon pulse. *Optics Letters*, 43(11):2644, 2018.
- [40] D. Yoshioka. *Statistical Physics: An Introduction*. Springer Berlin Heidelberg, 2006.
- [41] A. Zeilinger. General properties of lossless beam splitters in interferometry. *American Journal of Physics*, 49(9):882–883, 1981.